United States Department of Commerce
Technology Administration
National Institute of Standards and Technology

NIST Technical Note 1500–7
Materials Reliability Series

Structure–Property Relationships in Steel Produced in Hot-Strip Mills

P.T. Purtscher
Y.W. Cheng
C.N. McCowan

NIST Technical Note 1500–7
Materials Reliability Series

Structure–Property Relationships in Steel Produced in Hot-Strip Mills

P.T. Purtscher
Y.W. Cheng
C.N. McCowan

Materials Reliability Division
Materials Science and Engineering Laboratory
National Institute of Standards and Technology
325 Broadway
Boulder, Colorado 80303-3328

August 1999

U.S. DEPARTMENT OF COMMERCE, William M. Daley, Secretary
TECHNOLOGY ADMINISTRATION, Gary R. Bachula, Acting Under Secretary for Technology
NATIONAL INSTITUTE OF STANDARDS AND TECHNOLOGY, Raymond G. Kammer, Director

National Institute of Standards and Technology Technical Note
Natl. Inst. Stand. Technol., Tech. Note 1500–7, 72 pages (August 1999)
CODEN:NTNOEF

U.S. GOVERNMENT PRINTING OFFICE
WASHINGTON: 1999

For sale by the Superintendent of Documents, U.S. Government Printing Office, Washington, DC 20402-9325

Contents

Foreword v

1. Introduction 2
   1.1 Scope 2
   1.2 Relationship of the Commercial Product to the Experimental Models 3
   1.3 Project Justification 3
      1.3.1 Hot-Rolled Products 3
      1.3.2 Other Benefits 4
         1.3.2.1 Grade Consolidation 4
         1.3.2.2 Control Optimization for New Grades 4
         1.3.2.3 Cold-Rolled and Annealed Products 4
         1.3.2.4 Hot-Strip Mill Productivity 5
2. Structure–Property Goals 5
3. Structure–Property Approach 5
   3.1 Grain Refinement 7
   3.2 Dislocation Strengthening 7
   3.3 Transformation Strengthening 8
   3.4 Texture Strengthening 8
   3.5 Precipitation Strengthening 8
   3.6 Solid-Solution Strengthening 9
4. Results 9
   4.1 A36 Steel 9
      4.1.1 Through-Thickness Gradients and Nonpolygonal Microstructures 11
      4.1.2 Toughness 14
   4.2 DQSK Steel 16
   4.3 HSLA-V, 350 MPa Grade Steel 18
      4.3.1 Temper-Rolling 20
      4.3.2 Within-Coil Variations 20
      4.3.3 Influence of Test Orientation 21
      4.3.4 Aging of Coil Samples 22
   4.4 HSLA-Nb, 350 MPa Grade Steel 23
      4.4.1 Within-Coil Variations 27
      4.4.2 Aging of Coil Samples 28
   4.5 HSLA-Nb–Ti, 360 MPa Grade Steel without Excess Titanium 29
      4.5.1 Within-Coil Variations 30
      4.5.2 Aging of Coil Samples 30

4.6 HSLA-Nb–Ti, 550 MPa Grade Steel with Excess Titanium 30
4.6.1 Grain-Size Measurements 30
4.6.2 Coil-to-Coil Variation 31
4.6.3 Within-Coil Variations 33
4.6.4 Aging of Coil Samples 33
4.6.5 Effect of Heat Treatment 34
4.7 Nb–Ti and Niobium-Lean IF Grade Steel 34
4.8 Other HSLA-Nb Grade Steel 37
4.8.1 Within-Coil Variations 40
4.8.2 Aging of Coil Samples 40
4.9 Ferrite Grain-Size Measurements—Round Robin 41
5. Discussion 42
5.1 Equations to Predict Properties 42
5.1.1 Plain-Carbon Steel: Base Strength 42
5.1.1.1 Review of Equations in the Literature 43
5.1.1.2 Application to the Hot-Strip Model 45
5.1.2 HSLA Steel: Precipitation Strengthening 45
5.1.2.1 Review of Equations in the Literature 46
5.1.2.2 Application to the Hot-Strip Model 47
5.2 Fine-Tuning of Equations 49
5.3 Validation of Equations 50
5.3.1 Plain-Carbon Steel 50
5.3.2 HSLA Steel 52
5.3.2.1 HSLA-V Grade Steel 52
5.3.2.2 HSLA-Nb Grade Steel without Excess Titanium 53
5.3.2.3 HSLA-Nb–Ti Grade Steel with Excess Titanium 53
5.3.3 Validation from the Steel Companies 57
6. Additional Applications 61
7. Limitations 62
8. Summary and Recommendations 61
9. References 64

Foreword

The Materials Reliability Series of NIST Technical Notes are reports covering significant research accomplishments of the Materials Reliability Division. The division develops measurement technologies that enable the producers and users of materials to improve the quality and reliability of their products. Measurement technologies are developed for process control to improve the quality and consistency of materials, for nondestructive evaluation to assure quality of finished materials and products, and for materials evaluation to assure reliable performance. Within these broad areas of measurement technology, the division has focused its resources on three research themes:

- Intelligent Processing of Materials—To develop on-line sensors for measuring the materials' characteristics and/or processing conditions needed for real-time process control.
- Ultrasonic Characterization of Materials—To develop ultrasonic measurements for characterizing internal geometries of materials, such as defects, microstructures, and lattice distortions.
- Micrometer-Scale Measurements for Materials Evaluation—To develop measurement techniques for evaluating the mechanical, thermal, and magnetic behavior of thin films and coatings at the appropriate size scale.

This report is the seventh in the series. It covers research on structure–property relationships in steel produced in hot-strip mills, one of the projects on Intelligent Processing of Materials. Previous reports in this series are:

Technical Note 1500-1	Tensile Testing of Thin Films: Techniques and Results, by D.T. Read, 1997
Technical Note 1500-2	Procedures for the Electron-Beam Moiré Technique, by E.S. Drexler, 1998
Technical Note 1500-3	High-Energy, Transmission X-ray Diffraction for Monitoring Tubine-Blade Solidification, by D.W. Fitting, W.P. Dubé, and T.A. Siewert, 1998
Technical Note 1500-4	Nondestructive Characterization of Reactor Pressure Vessel Steels: A Feasibility Study, by H.I. McHenry and G.A. Alers, 1998
Technical Note 1500-5	Electron-Beam Moiré Technique: Advances, Verification, Application, by E.L. Drexler, 1998
Technical Note 1500-6	Constitutive Behavior Modeling of Steels under Hot-Rolling Conditions, by Y.W. Cheng, R.L. Tobler, B.J. Filla, and K.J. Coakley, 1999

Structure–Property Relationships in Steel Produced in Hot-Strip Mills

Patrick T. Purtscher, Yi–Wen Cheng, and Chris N. McCowan

Materials Reliability Division
National Institute of Standards and Technology
Boulder, CO 80303

The purpose of this work was to develop equations for the Microstructural Engineering–Hot-Strip Mills project that predict the mechanical properties of steel produced in hot-strip mills as functions of chemical composition and microstructural variables, such as ferrite grain size and fraction, at ambient temperatures *after* hot-rolling. Data for eight steel grades, A36, DQSK (drawing quality special killed), HSLA-V, HSLA-Nb, HSLA-50/Nb–Ti, HSLA-80/Nb–Ti and two interstitial-free grades, produced by three different companies, were used to evaluate the equations.

To develop and evaluate the equations, mill-produced products were supplemented by laboratory-produced samples. For the plain-carbon grades (A36 and DQSK), the laboratory-produced samples provided a wider range of microstructural variables than those supplied by the mills. For the high-strength, low-alloy (HSLA) grades, the laboratory treatments were successful in simulating the precipitation-coarsening kinetics only.

Equations to predict the yield strength, ultimate strength, and total elongation for the eight steel grades have been developed and were used in the hot-strip mill model (HSMM). For A36, an equation to predict the ductile-to-brittle transition temperature in the Charpy impact test is also given. The equations' predictions correlate well with the available experimental data, indicating that the equations adequately describe the properties of the eight steel grades that were considered. The equations' predictions for strength in plain-carbon steel were further validated with data obtained from one manufacturer. To demonstrate the application of the equations to other HSLA grades, the predicted strength properties of HSLA steel were compared with those obtained from similar niobium-containing grades from two other producers.

The equations have been used, along with the separate thermal, rolling, transformation, and coiling models, to calculate the properties in the HSMM developed at the University of British Columbia in Canada. The accuracy of the mechanical property predictions critically depends upon the accuracy of the thermal and transformation models' predictions.

Key words: grain size; hot-strip rolling; HSLA steel; mechanical properties; plain-carbon steel; precipitation strengthening.

1. Introduction

1.1 Scope

This research project was proposed in 1992 to enhance the competitiveness of American Iron and Steel Institute (AISI) member companies by developing a predictive tool that could quantitatively link the properties of hot-rolled steel products to the process parameters of a hot strip mill. It is part of an overall advanced process-control program operated through AISI with the majority of the funding provided by the U.S. Department of Energy. The scope of the program, excerpted from the initial proposal (1992) follows.

> The predictive tool would be a user-friendly computer model that incorporates heat flow, knowledge of microstructural phenomena (recrystallization, grain growth, precipitation, and austenite decomposition), and structure–property relationships, to compute the thermal and microstructural evolution of steel during hot-rolling, as well as final product properties (at the downcoiler), as a function of hot-strip mill design and operating practice. This project focuses on the heart of the competitiveness issue—the linkage of product and process. This project will concentrate on difficult, property-critical microalloyed (niobium- and vanadium-bearing) steel grades and will be unique in its capability compared with counterparts that have been under development in countries such as Japan, England, Australia, and Canada. *Owing to its fundamental knowledge base, the model will have universal applicability and will be capable of expansion to include a wide variety of steel grades.*
>
> Development of the model will follow well-established principles of microstructural engineering involving computer programming, quantitative characterization of the kinetics of the different microstructural phenomena, measurement of surface heat extraction in the different zones of the hot-strip mill (scale breakers, rolls, interstand coolers, and runout table) and other experimental work in the plant and pilot plant to obtain steel samples (slabs, transfer bar, and coil), roll-separating forces, and temperature measurements for model verification.
>
> Each of the microstructural engineering activities will be based upon earlier work, the experience of the individuals in the research team, and established experimental facilities. The computer model will be built upon models that have been developed to predict the thermal evolution and change to austenite grain size in the roughing and finishing sections of a hot-strip mill, as well as the deformation of the work piece in the roll bite (strain, strain-rate distributions), which permits calculation of the roll separating force. In addition, a newly developed coiling model is a part of the effort. These models will be integrated into an overall predictive tool that is user friendly.
>
> The major thrust of the project is the research to characterize the kinetics of the microstructure phenomena together with the constitutive behavior and structure–property relationships of the steel grades under study. The National Institute of Standards and Technology (NIST) will develop the constitutive equations to predict the basic material response at rolling temperatures and the structure–property equations at ambient temperatures. The University of British Columbia (UBC) is responsible for the computer modeling and various physical-metallurgy investigations (grain growth, recrystallization, precipitation, and transformation). The steel to be investigated will primarily include microalloyed grades (containing niobium and/or vanadium) in two carbon ranges, 0.07 % to 0.09 % and 0.17 % to 0.20 %.

A summary of the existing and emerging technology revealed that substantial modeling exists in a qualitative state, with the exception of the coiling model. This project proposed extensive physical metallurgy research and experimentation to develop quantitative models for property-critical microalloyed hot-rolling grades. The process models developed at UBC included the roughing mill, finishing mill, runout table, and coiling; the constitutive properties at hot-working temperature and the structure–property relationships at room temperature were determined at NIST. Prior work in C–Mn steel formed the basis of some of the individual modeling of hot-rolling, but the integration effort, the particular grades we were working on, and the physical metallurgy behind the resulting quantitative model made this work both challenging and unique. The project included linking the quantitative models to produce a deliverable project that would accurately predict the properties of microalloyed hot-rolled grades.

1.2 Relationship of the Commercial Product to the Experimental Models

In this project, the involvement of the commercial partner was critical because a high degree of flexibility had to be designed into the software product for it to be useful to the industry as a whole.

Many coefficients and parameters were necessary for the proper operation of the integrated model. These parameters were based on physical metallurgy principles, although there was an element of site influence. Determining the coefficients at a given site was not the problem because extensive operating data are available. (Hot-strip mills are among the most instrumented of steel producers.) The problem was to ensure that the model enables simple editing of these items by the user. All coefficients and parameters had to be adjustable for the different configurations at different companies. It was not sufficient to wait until the model was proven and then build in the flexibility during commercialization, because this would prolong the commercialization phase. Our design of model experiments minimizes the amount of modification necessary during commercialization.

1.3 Project Justification

The production of hot-strip mill products with specific mechanical properties or with specific microstructural attributes currently requires numerous and costly full-production trials before both the ranges of chemical composition and of hot-strip mill processing parameters can be comfortably defined. However, the basic components of current technology enable the calculation of austenite microstructural development and refinement during hot-rolling as a function of workpiece composition, temperature, starting microstructure and deformation strains, and strain rates. In addition, austenite transformation can be described mathematically as a function of steel composition, prior austenite microstructure, and thermal path during cooling. Such microstructural calculations, as a function of thermomechanical processing history, could be coupled with established microstructure–property relationships so that final mechanical properties could be predicted as a function of steel composition and thermomechanical history. In addition to the use of the proposed microstructural model for hot-strip mill products, it is clear that the hot-strip mill model (HSMM) could be readily adapted to other hot-working operations; in particular, it could be directly applied to plate-mill rolling by simply using the appropriate modules in the model.

1.3.1 Hot-Rolled Products

Manufacturing hot-rolled products with a given initial range of properties is desirable for hot-rolled products that receive no significant further processing or those with well-characterized property changes due to fabrication. The production of high-strength, hot-rolled sheet products to specific levels and to very tight ranges of mechanical properties requires that rolling and cooling conditions be varied

from slab to slab as minor changes in steel composition and/or processing temperatures are encountered. In addition, hot-rolled bands that are converted to tubing or electric-resistance welded pipe generally require minimum levels of Charpy-impact notch toughness in addition to minimum strength levels, and microstructural control is essential for the development of proper balance of grain size, solid-solution strengthening, and precipitation strengthening. Further, hot-strip mill plate products (plate-type products rolled on the hot-strip mill rather than on a plate mill), such as A36 and A572, grade 50 steel, must also be produced with minimum strength and toughness levels, which are controlled by microstructure. Hot-rolled and controlled plate products are also produced to similar strength and toughness requirements where control of microstructure is critical. Twenty-two million tons of steel are produced annually in North American hot-strip mills.

1.3.2 Other Benefits

1.3.2.1 Grade Consolidation

The numerous grades normally produced in the steel-making shop (continuous cast to slab form, inventoried ahead of the hot-strip mill or plate mill, and finally rolled to finished product) could be combined. Combination of grades would require computational techniques that could adjust the processing variables for a given composition to produce various fixed sets of properties rather than having a different composition for each mechanical property requirement. The reduction in the number of steel compositions within a steel plant would have significant positive economic effects.

1.3.2.2 Control Optimization for New Grades

When a new steel grade is rolled on a hot-strip mill or plate mill, a significant learning curve is encountered as the computer control system "learns" what to expect of this new steel grade and develops a set of internal tables (such a hardness curves) within its memory for subsequent rolling of this product. If force and microstructural models were available as a function of steel composition, a significant reduction in this learning time and associated cost savings would be realized. Further, lowering of slab reheating temperatures is more feasible for plate-mill than for strip-mill processing, and consequently, energy savings could be realized.

1.3.2.3 Cold-Rolled and Annealed Products

For hot-rolled coils that will be subjected to subsequent processing, particularly cold reduction and annealing, it is normally desirable to produce the hot band with specific microstructural attributes that are necessary to optimize properties after the subsequent processing steps. In other words, producing the optimum properties off the hot-strip mill will enable tighter, more efficient control of properties in cold-rolling and annealing.

With the reduction in carbon and nitrogen contents in such grades as interstitial-free (IF) and bake-hardening steel, the control of interstitial and/or precipitated nitrogen and carbon atoms is essential for determining of the final properties of the annealed sheet products. Thus, microstructural control on a submicroscopic scale is necessary in these cold-rolled products, and such control begins on the hot-strip mill, starting with slab reheating and finishing with coiling. Although this aspect of the modeling process may present the greatest challenge, the understanding and control of these precipitate dissolution and re-precipitation reactions through application of transformation and coiling modules will produce significant benefits in controlling the level and uniformity of cold-rolled strip products.

1.3.2.4 Hot-Strip Mill Productivity

Mill productivity is partially limited by the maximum acceleration or zoom rate that is imposed on the mill to maintain a relatively constant finishing temperature. However, productivity could be improved by reducing the time required for any given bar in the finishing train, which might be possible (1) if the finishing temperature could be allowed to increase and the runout table cooling could be modified to give a variable coiling temperature with constant properties in the finished coil or (2) if interstand strip cooling could be introduced to maintain a constant finishing temperature. The model would enable off-line calculation of potential scenarios and development of advanced control strategies. Such improved throughput on the hot-strip mill would be applicable to all product lines. In addition, by considering different profiles (other than constant) for the coiling-temperature trace for a given coil, end effects at the head and tail of coils could be minimized, and, consequently, the yields would increase.

2. Structure–Property Goals

This report summarizes the work related to development of structure–property equations at ambient temperatures for steel rolled in hot-strip mills (a subtask in the overall program). Three main technical hurdles associated with this subtask are

- characterization of fine, sometimes complex microstructural features
- development of non-process-specific constants in the equations
- relating the other subtasks to the proposed structure–property equations, including verification of the predictions from the computer program with mill data

The responsibility for the first two hurdles is self-contained within the subtask and is reported on here. Responsibility for the third hurdle is ultimately shared among the partners in the program (NIST, UBC, and the AISI members) and can be only partially evaluated with the information currently available at this time.

3. Structure–Property Approach

Good room-temperature mechanical properties, such as yield strength (YS) and (ductile-to-brittle transition temperature (DBTT), are requirements for many hot-rolled steel products. These properties are usually related to product composition and ferrite grain size. Empirical equations, based on principles of physical metallurgy that relate properties to composition and grain size, are widely available for the air-cooled C–Mn steel. However, for high-strength, low-alloy (HSLA) steel, the correlation of structure and properties has not been well-characterized in the literature.

Lack of good physical models to represent a given mechanical property is another problem related to the development of structure–property equations based on physical metallurgy principles. The simplest mechanical property of interest would be YS, but even here, there are complications. The yield-point elongation (YPE) can vary significantly, depending upon the ferrite grain size and the volume fraction of the second phase, and it will change the measured lower YS (LYS); yet no approach to separate the microstructural dependence of YPE from the true structural dependence of YS exists.

The basis of most equations for structure–property relationships is the assumption that the different mechanisms responsible for the properties can be described individually by the composition and microstructure and that the effects of each are additive. For example, the YS has been described as a sum of the strength contributions from different mechanisms—grain refinement ($k_y \times d^{-0.5}$), dislocation σ_{disl}, transformation σ_{tr}, texture σ_{tex}, precipitation σ_{ppt}, and solid solution σ_{ss}—as shown below:

$$YS = \sigma_0 + k_y d^{-0.5} + \sigma_{disl} + \sigma_{tr} + \sigma_{tex} + \sigma_{ppt} + \sigma_{ss}, \quad (1)$$

where σ_0 is assumed to represent the lattice friction for pure iron. This approach makes the implicit assumption that the contributions from the different mechanisms are additive. This assumption is useful from a practical point of view, and it is the approach taken in most studies. Experiments in which the strengthening mechanisms were not additive have been reported [1].

Examples of some of the equations to predict the ultimate tensile strength (UTS) of steel found in the literature are shown in table 1 [2–7]. Several variations on the basic approach are evident. Several groups tried to predict the hardness of the individual microstructural components from the transformation temperatures and then inferred the UTS from hardness. Processing parameters, such as the cooling rate,

Table 1. Summary of UTS predictions found in the literature for steel.

Investigator	Ultimate tensile strength, MPa
Pickering [2] 1977, England	$UTS = 294 + 27.7[Mn] + 83.2[Si] + 385X_p + 7.85d^{-1/2}$
Choquet et al. [3] 1990, France	$UTS = UTS_0 + UTS_{ss} + 7.24X_\alpha d^{-1/2} + 500X_p$ $UTS_0 = 237;\ UTS_{ss} = 29[Mn] + 79[Si] + 700[P] + 5369[N_{free}]$
Suehiro et al. [4] 1988, Japan	$UTS = 3.04\ H_v$, where $H_v = X_\alpha H_\alpha + X_p H_p + X_b H_b$; $H_\alpha = 361 - 0.347T_m^\alpha + 50[Si];\ H_p = 175;$ $H_b = 508 - 0.588T_m^b$
Mitchell et al. [5] 1993, England	$UTS = 74.1 + 985.1CEV + (31125[N_{free}] - 39)[V]^{1/2} + 181.5t^{-1/2}$ where $CEV = [C] + [Mn]/6 + \{[Cr] + [Mo]\}/5 + \{[Ni] + [Cu]\}/15$
Kwon [6] 1992, Korea	$UTS = 0.095X_\alpha H_\alpha + 0.264X_p H_p + 0.277X_b H_b + 11d^{-1/2}$ $+ 75.5X_\alpha d^{-1/2} + 13.4\ X_\alpha(1 - X_\alpha) + 3.8$ where $H_\alpha = 27.72\ \exp(980/T_m^\alpha) + 39.8[Si] + 9.1$ $H_p = 215.4 - 0.016T_m^p - 34.04[Mn] + 58.26[Si]$ $H_b = 27.72\ \exp(980/T_m^b) + 39.8[Si] + 9.1$
Hodgson and Gibbs [7] 1992, Australia	$UTS = 164.9 + 634.7[C] + 53.6[Mn] + 11d^{-1/2}$

X_α, X_p, and X_b = volume fraction of ferrite, pearlite, and bainite
d = ferrite grain size in millimeters
H_v = Vickers hardness number; H_α, H_p, and H_b = Vickers hardness for ferrite, pearlite, and bainite
T_m^α and T_m^b = average transformation temperature in degrees centigrade for ferrite and bainite
$[N_{free}]$ = [N] – 3.42[Ti]
t = thickness of plate in millimeters

were sometimes used as input. Several researchers have specifically incorporated precipitation strengthening into their predictions but without the use of the related microstructural features like the particle size and spacing between particles. The carbon equivalence (CEV) was used in one case to describe the solid-solution strengthening where welded applications are of interest. An alternative and more rigorous approach to predict UTS (not shown in table 1) has been proposed by Tomota et al. [8]: the entire stress–strain curve is predicted, and the UTS is given by the point where the true flow stress is equal to the strain hardening rate.

For this project, we incorporated some of the details of the different approaches that seem to work best for our intended goal. In the next sections, the individual components of the equations are discussed briefly with respect to this project.

3.1 Grain Refinement

Grain size is a critical factor influencing YS; grain size is also the most important parameter that can change with different processing routes in the hot-strip model to enable the predicted property to change. Yet no physical model for the interaction between grain size and YS has been proposed and validated for the type of ferritic sheet steel that we were studying. Mintz [9] has discussed the importance of the grain-size dependence (Hall–Petch slope k_y) in determining YS of steel and summarized the literature on this subject. Variations in k_y for commercial compositions range from a low of 14 MPa × $mm^{0.5}$ to a high of 24 MPa × $mm^{0.5}$. When all the carbon and nitrogen are removed from solid solution, values as low as 5 MPa × $mm^{0.5}$ to 6 MPa × $mm^{0.5}$ have been reported. Physically, the variation is almost certainly related to segregation of interstitial atoms to grain boundaries, which increases the stress needed to nucleate new dislocations from the boundary regions. In practice, the variations in k_y do not translate into significant differences in the predicted YS because there are systematic changes in σ_0 that counteract the variations in k_y. Part of the variation in k_y is also related to how grain size is measured. This factor has been discussed in more detail by Gladman and Pickering [10].

The grain size dependence of the UTS is certainly less than that of YS. In the equations for YS and UTS proposed by Hodgson and Gibbs [7], the factors are 19.7 MPa × $mm^{0.5}$ and 11 MPa × $mm^{0.5}$. Pickering [2, 11] used 15.1 MPa × $mm^{0.5}$ and 7.7 MPa × $mm^{0.5}$ for k_y in his equations for YS and UTS. In both cases, the dependence of YS on grain size is about twice that for UTS. Campbell et al. [12] have proposed a different trend where the k_y for YS is 11.8 MPa × $mm^{0.5}$ and for UTS, 15.9 MPa × $mm^{0.5}$. The fact that equations from different sources predict different trends in a given property reflects more upon the database used to generate the equations than any fundamental characteristic of the steel's behavior.

The predictions from the equations in this report for elongation and DBTT are a strong function of ferrite grain size, but the equations are derived mainly from literature reports rather than developed from our own data base. For total elongation, the prediction varies with the UTS.

3.2 Dislocation Strengthening

Dislocation strengthening has little influence on properties of most hot-rolled, low-carbon sheet steel because the mill conditions (finishing and coiling temperatures) are such that the structure is usually polygonal ferrite, which is free of excess dislocations. With higher carbon content, larger austenite grain size, and high local cooling rates, nonpolygonal transformation products can form and excess dislocations are an issue for property prediction. The presence of excess dislocations in the structure (ones that affect the prediction of properties) can be difficult to detect. Often, light microscopy can provide only hints

as to the dislocation content. The best way to characterize dislocations is transmission electron microscopy (TEM), but difficulties in sample preparation and quantitative interpretation of TEM results limit its use for model development.

For our project, A36 and HSLA-Nb–Ti are the only grades where nonpolygonal microstructures are important and then only for specific processing routes. Literature data [13] suggest that some modifications to the equations for polygonal ferrite microstructure are necessary to describe the strength of the nonpolygonal microstructures. For the limited conditions under which dislocation strengthening is relevant, we have modified the strength equations used for polygonal structures to reflect the change in strength due to the nonpolygonal microstructures. The total elongation is assumed to be influenced only by the relative change in UTS. Predictions for the DBTT are not changed by the nonpolygonal structure because we did not have any database to quantify the effects.

3.3 Transformation Strengthening

Transformation strengthening is one area of the program where it is difficult to separate the individual models within the HSSM. The equations that describe transformation and the structure–property equations are intimately related. For example, the equations for strength from Campbell et al. [12] require a pearlite spacing, but the transformation model does not predict that level of detail. The transformation model developed at UBC takes into consideration the steel grade (not exact composition), austenite grain size, cooling rate, and transformation heat. The output of the model gives ferrite fraction, ferrite grain size, and the microalloy content in solution at the transformation temperature.

3.4 Texture Strengthening

Texture plays an important role in the ductility and forming properties of steel, but it has only a minor role in determining the strength of the final product. Typically, texture contributes about 30 MPa to strength [11], with the transverse properties higher than the longitudinal properties. The influence of texture on total elongation is assumed to be represented by the predicted change in UTS. The prediction of the other properties is unaffected by texture.

3.5 Precipitation Strengthening

Precipitation strengthening refers to the increase in strength that is associated with the formation of small particles of a second phase in a matrix, where the elements that make up the particles were initially dissolved in the matrix. Precipitation is a minor factor for plain-carbon steel (AlN precipitation determines the free nitrogen content that contributes to solid-solution strengthening); however, it is important in HSLA steel. When a steel is alloyed with niobium, titanium, and/or vanadium, microalloy carbonitrides can precipitate in austenite and/or ferrite. Precipitation in austenite retards recrystallization and grain growth and also increases the deformation resistance of the steel. With regard to the mechanical properties at ambient temperatures, precipitation in austenite is generally assumed to limit the amount of alloying elements available to form precipitates in ferrite, which increases the measured mechanical properties. Precipitation strengthening in ferrite is controlled by the volume fraction of the particles and the coarsening of precipitates; the volume fraction of particles can be estimated from the chemical composition, but information on the kinetics of carbonitride coarsening in ferrite is absent from the literature. A major part of our effort has been to characterize the kinetics for precipitates that form in ferrite. These precipitates are mostly carbonitrides with niobium, niobium–titanium, or vanadium.

Table 2. Element vectors for structure–property relationships (MPa/mass %) in commercial C–Mn and microalloyed steel.

Element	Hodgson and Gibbs [7]		Choquet et al. [3]		Pickering [2]	
	LYS	UTS	LYS	UTS	LYS	UTS
Mn	26.1	53.6	23	29	37	27.7
Si	60.2	99.7	53	79	83	83.2
P	759	651.9	700	700	680	—
Cu	212.9	—	—	—	38	—
Ni	—	472.6	—	—	33	—
N	3286.0	3339.4	5000	5369	5000	—

3.6 Solid-Solution Strengthening

Solid-solution strengthening has been studied extensively, and it is widely accepted that the solid-solution strengthening adds to the lattice friction in eq (1). Theory and experiment have shown that the increase in strength is proportional to the square root of the concentration of the solute atom. For dilute solutions, such as low-carbon sheet steel, a linear relationship is generally assumed. The exact value of the strengthening coefficients varies from one study to the next. The values published for LYS and UTS from three different sources are shown in table 2. The differences are significant and again reflect the different databases from which the equations were developed. The property predictions from the different sources are similar because the differences tend to cancel for the compositions typically encountered. Problems will almost certainly arise if the equations are applied outside of the range of compositions in the database for which each was developed.

4. Results

4.1 A36 Steel

A summary of all the tensile tests along with the microstructural characterization [equivalent grain diameter (EQAD) and ferrite fraction, f_α] is shown in table 3. Both as-received coil and heat-treated samples are included. The microstructure of the thinnest A36 coil is shown in figure 1. Grain size and ferrite fraction change with the processing conditions. The ferrite grain size for the five coils received from one steel producer (shown in the table) varied from 5×10^{-3} mm to 6.5×10^{-3} mm, whereas the ferrite fraction varied from 0.87×10^{-3} mm to 0.81×10^{-3} mm. The major unknown factor in the microstructure relates to the second phase. Locally, the second phase can be more than 0.4 mm from the top surface, and the grains are less polygonal when the section size is greater than 6 mm. Additional tests were performed to evaluate the influence of microstructure in thicker products (>10 mm thick) on the DBTT in this grade. Laboratory processing of A36 was a very valuable procedure to expand the range of microstructures to be evaluated in the mill samples.

Table 3. Summary of tensile tests on A36 steel coils.

Coil number	Gauge, mm	Location[a]	Coiling temp., °C	EQAD, mm	f_α	YS, MPa	UTS, MPa	Elong., %
1	9.4	MC	665	5.4×10^{-3}	0.81	285	445	30
2	6.1	MC	669	5.0×10^{-3}	0.85	312	474	34.5
3	9.1	MC	685	5.5×10^{-3} (6.5×10^{-3})	0.85	277	426	39.5
4	4.8	MC	684	6.5×10^{-3} (5.5×10^{-3})	0.87	319	457	37
5	4.3	HC	688	5.9×10^{-3}	0.86	315	442	36
5	4.3	TC	688	6.2×10^{-3}	0.87	302	455	34
5	4.3	b	915[c]	12.0×10^{-3}	0.80	257	393	39
5	4.3	b	915[d]	7.6×10^{-3}	0.80	313	428	34

[a] MC = middle center; HC = head center; TC = tail center

[b] laboratory heat-treated

[c] reheat temperature followed by furnace cooling

[d] reheat temperature followed by air cooling

Figure 1. Typical microstructure for A36 steel. Bar in picture represents 10×10^{-3} mm.

4.1.1 Through-Thickness Gradients and Nonpolygonal Microstructures

The A36 grade presented some different problems because it has the highest carbon content of any of the grades in the program and because the samples received from the mill covered a wider range (approximately 4 mm to 10 mm) in thickness. For the thickest coil, there was a gradient in the microstructure; the top surface exhibited nearly all nonpolygonal ferrite grains and the center and bottom surface exhibited polygonal grains. Figure 2 shows the appearance of the second phase in a 9.7 mm thick sheet, near the top surface and in the middle. The properties of the pearlite with its lamellar carbides found in the middle are well-characterized in the literature; the properties of the patches of degenerate pearlite or bainite found near the top are not. Hardness profiles through the thickness of the two thickest coils are shown in figure 3, and quantitative metallography from the thickest coil is shown in figure 4. These variations are produced in the hot strip mill because the top surface of a thick plate cools faster. (A sheet of water tends to cover the top surface and promotes better heat transfer.)

For the prediction of properties in the case where there is a gradient in microstructure, the following guidelines have been adopted: The cross-section is divided into 100 evenly spaced points; each point is assigned specific values for temperature and ferrite grain size and fraction by the HSMM. The HSMM divides the cross section into quarters, and the YS for the coil is taken to be the lowest average YS for any quarter, whereas the UTS for the coil is simply the average of all points.

A complication resulting from a steep thermal gradient through the thickness is that low-temperature, nonpolygonal transformation products like bainite or martensite can form near the surface of the coil on the runout table. The subsequent coiling temperature can be higher than the transformation temperature. This type of complication will temper the nonpolygonal structure, changing its strength.

A modification to the equations for A36 has been developed to decrease the predicted mechanical properties of the nonpolygonal microstructures found near the top surface of coils with a thickness greater than 6 mm. Figure 5 shows data for 1016 steel (carbon content is 0.16 %, manganese content is 0.75 %) taken from the literature [14]. For three cooling conditions that produce microstructures containing bainite, the as-quenched hardness is shown to be reduced after tempering at temperatures between 500 °C and 700 °C. The ratio of tempered hardness to as-quenched hardness changes at nearly a constant rate for the temperature range of interest, that is, the temperature at which the strip is coiled.

Without a correction to the properties for coiling temperature, the model for A36 predicts strength properties that are higher than expected for those regions of the coil with nonpolygonal microstructures. Given this limited set of data for 1016 steel that has nearly the same composition as A36, we suggest that the predicted properties be modified to reflect the influence of coiling temperature in a similar fashion. Therefore, whenever the local transformation temperature is lower than the coiling temperature, the model will need to multiply the current strength predictions by a factor Φ that varies from about 0.9 to 0.72, depending on the coiling temperature within the range of 500 °C to 700°C. Given the limited amount of data on which this modification is based, a linear dependence of Φ on coiling temperatures between 500 °C and 700°C seems appropriate.

(a)

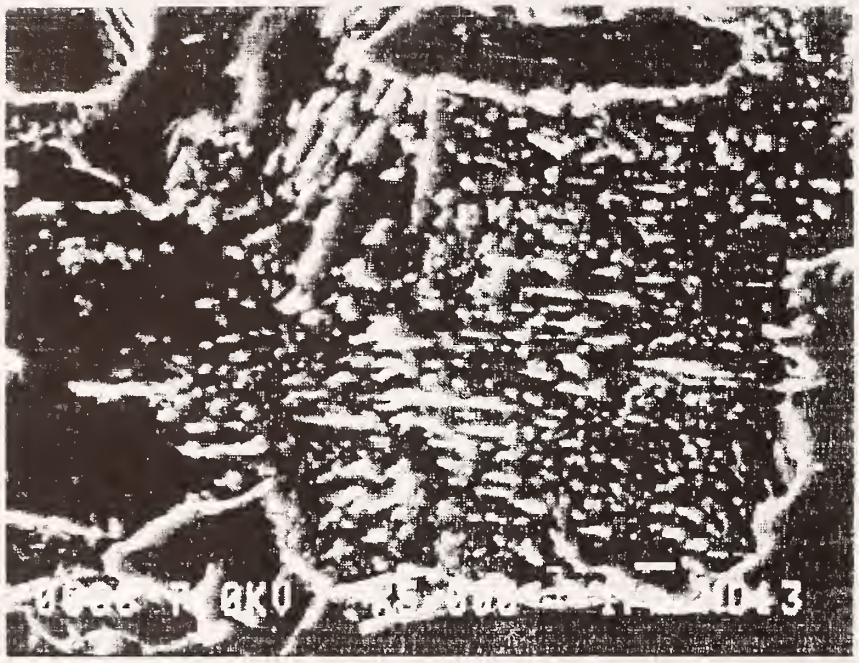

(b)

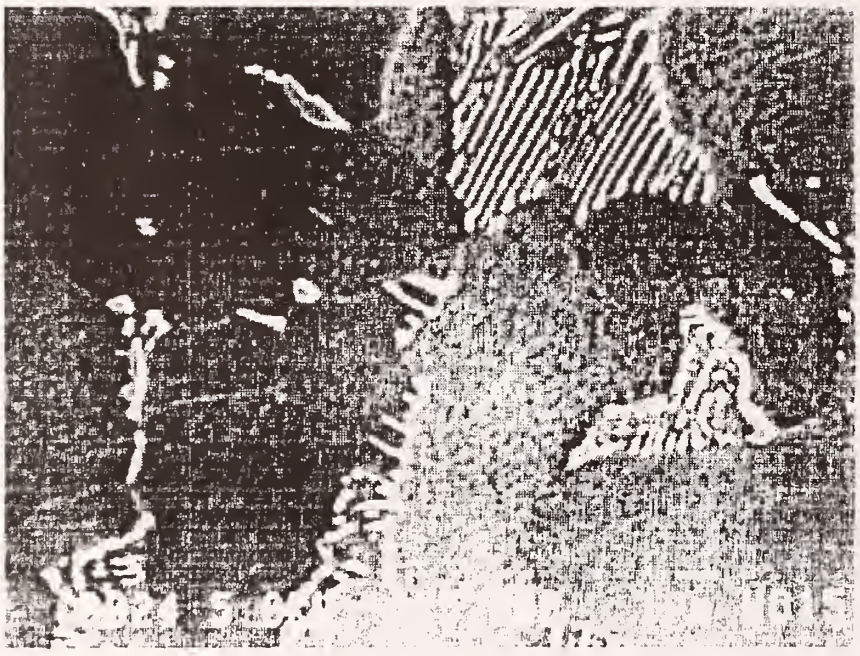

Figure 2. A36 microstructure found in as-received coil, 9.7 mm thick, (a) near top surface and (b) middle of cross section.

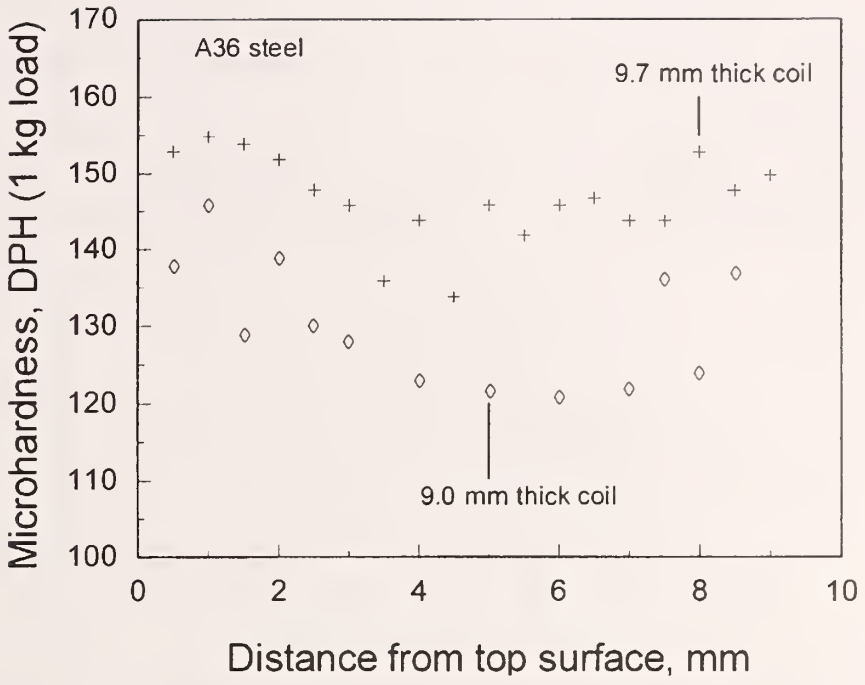

Figure 3. Hardness profiles through the two thickest A36 coils.

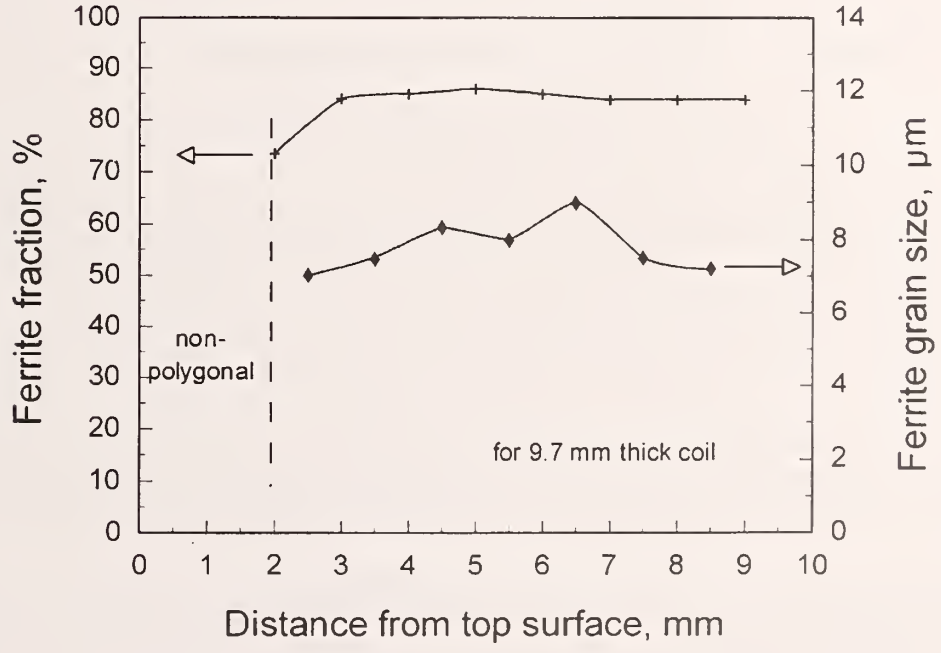

Figure 4. Quantitative metallography from the thickest A36 coil as a function of location through the thickness of the sheet.

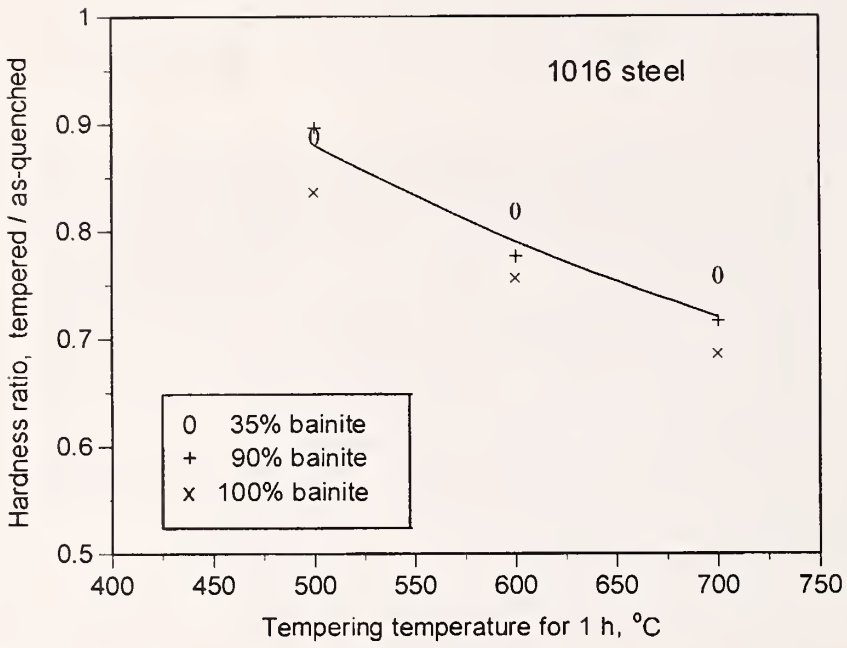

Figure 5. Ratio of tempered hardness to as-quenched hardness for 1016 steel as a function of tempering temperature.

4.1.2 Toughness

To predict toughness, Pickering [11] used the following equation:

$$\mathrm{DBTT} = -19 + 44\mathrm{Si} + 700\mathrm{N}_{\mathrm{free}}^{1/2} + 2.2f_p - 11.5d^{-1/2} \qquad (2)$$

where DBTT is in degrees centigrade, the compositions are in mass percent, f_p is the pearlite fraction, and the grain diameter d is in millimeters. To verify the equation's prediction, we tested A36 in two conditions. Thermomechanical processing was performed on A36 crop samples (30 mm thick) to provide samples for toughness evaluation. The blanks for processing were 80 mm long with a cross section of 13 mm × 30 mm. The blanks were soaked at 1100 °C for 10 min, furnace-cooled to the deformation temperature, deformed, cooled rapidly (about 50 °C/s at the surface) to about 700 °C, and then air-cooled. The deformation conditions and the resulting microstructural characterization are summarized in table 4. Results from tensile testing are summarized in table 5. Figure 6 shows the results of the Charpy V-notch tests. The relationship between the measured transition (27 J was used) and the transition predicted from Pickering's equation is shown in figure 7. The difference between measured and predicted values is 5 °C.

The effect of the nonpolygonal transformation product on toughness is not clear. Acicular ferrite and tempered bainitic microstructures can have relatively good toughness; however, the effects of grain refinement and alloy additions for nonpolygonal microstructures have not been systematically studied.

Table 4. Summary of processing and resulting microstructure for toughness samples (A36 crop).

Condition	Deformation temperature, °C	Strain	Ferrite grain size, mm	Pearlite content, %
A	1000	0.90	8.4×10^{-3}	30
B	1050	0.26	11.0×10^{-3}	30

Table 5. Summary of tensile properties for the toughness samples (A36 crop).

Condition	YS, MPa	UTS, MPa	Uniform strain, %	Reduction of area, %
A	317	467	22	67
B	270	450	17	68

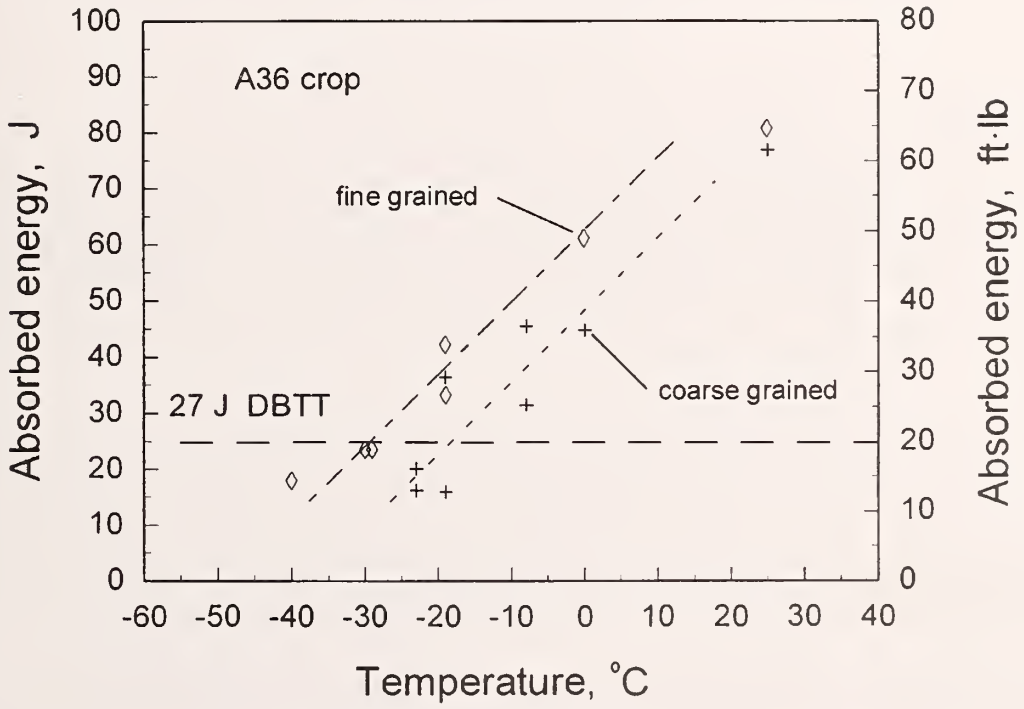

Figure 6. Charpy V-notch test results from A36 after thermomechanical processing.

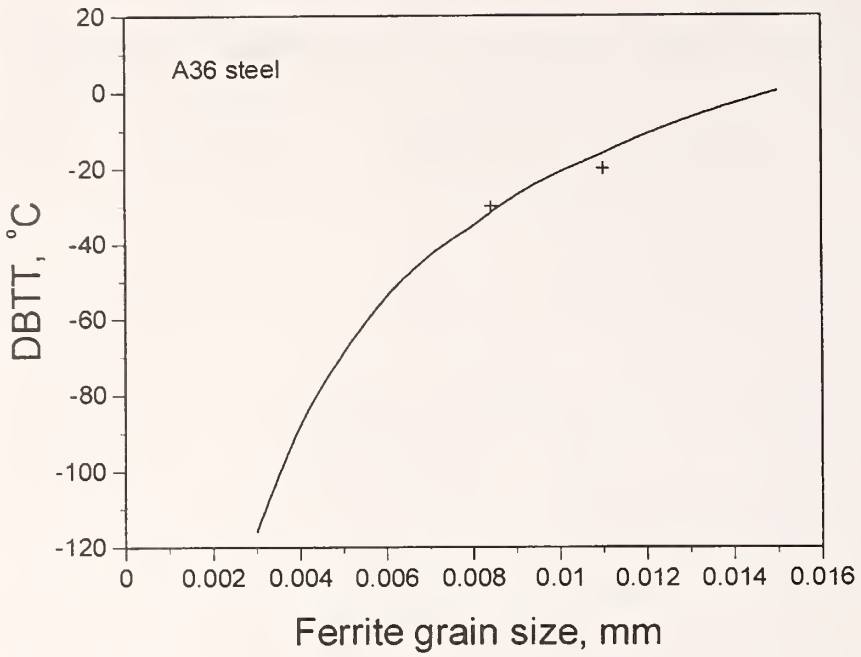

Figure 7. Comparison between equation predictions and measured values for the DBTT in A36 after thermomechanical processing.

4.2 DQSK Steel

A summary of all the tensile tests is shown in table 6. Both as-received coil and heat-treated samples are included. Figure 8 shows the microstructure that is typical of DQSK steel. Grain size and properties changed with processing conditions, but the ferrite fraction was relatively constant. The grains were polygonal, and little second phase was present. The ferrite grain size for the four coils (shown in table 6) varied from 8×10^{-3} mm to 10×10^{-3} mm, and the ferrite fraction was assumed to be 0.97. Laboratory processing of DQSK expanded the range of microstructures to be evaluated.

The changes in YS and UTS cannot be attributed solely to the variation in ferrite grain size; we expect that the dissolved interstitial content is the other significant factor that determines the properties. Carbon and nitrogen are interstitial alloying elements that have a large solid-solution strengthening effect (about 50 MPa per 0.01 %) when they are dissolved in the matrix. For hot-rolled strip with typical coiling conditions, we assumed that the carbon was completely tied up as Fe_3C. There is usually more than enough aluminum to combine with all of the nitrogen; however, we know that with a low coiling temperature, such as 550 °C, most of the nitrogen remains in ferrite and does not precipitate out as AlN.

To evaluate the content of free nitrogen, we performed a series of strain-aging tests where the samples were pulled in tension to a strain of 5 % and then aged in boiling water for 4 h before resuming the tension test. Table 7 shows these results. The aging index (increase in flow stress due to precipitation of carbides on the newly formed dislocations) was about 50 MPa for all the as-received coil samples and was zero for the laboratory-annealed samples. Our results can then be taken to indicate that there is at least 0.01 % free nitrogen in all the as-received samples, but an absolute value cannot be estimated. A torsion-pendulum test would be required to obtain better experimental data.

An existing model for AlN formation found in the literature has been adopted in the coiling module to calculate free nitrogen [15]. The calculation assumes that aluminum diffusion in ferrite controls the precipitation. The model was not validated because the temperature predictions in the coiling model and the free nitrogen content in the sample could not be verified.

Table 6. Summary of tensile tests on DQSK.

Coil number	Coil temp., °C	Measured YS, MPa	Measured UTS, MPa	Grain size, mm
1	665	320	390	7.9×10^{-3}
2	550	310	375	9.4×10^{-3}
3	550	244	335	10.4×10^{-3}
4	550	245	331	10.3×10^{-3}
1	915[a]	259	325	13.1×10^{-3}
1	950[a]	254	318	15×10^{-3}

[a] reheat temperature followed by air-cooling

Figure 8. Typical microstructure for DQSK steel. Bar in picture represents 10×10^{-3} mm.

Table 7. Summary of strain-aging experiments on DQSK steel coils.

Coil number and location	YP, MPa	YS, MPa	UTS, MPa	YP elong., %	Uniform elong., %	Total elong, %	Aging index,[a] MPa
1 – head middle	368	330	—	2.8	—	—	46
1[a] – head middle	346	321	—	4.9	—	—	0
2 – tail left edge	282	269	—	2.6	—	—	46
2 – tail center	322	277–321	375	2.7	18	29	54
2[b] – tail center	280	267	—	5.0	—	—	0
3 – tail left edge	253	253	339	2.3	23.8	35.3	52
3 – tail center	266	252	332	3.2	25.8	37	52
3[b] – tail center	256	253	—	5.5	—	—	0

[a] strained 5 % and then immersed in boiling water for 4 h
[b] annealed at 650 °C for 1 h before strain-aging test

4.3 HSLA-V, 350 MPa Grade Steel

A summary of all the tensile tests is shown in table 8. Both as-received coils and heat-treated samples are included. The mechanical properties of the as-received samples show a 50 MPa variation in YS and a 45 MPa variation in UTS. Figure 9 shows the microstructure that is typical of this grade. The grain shapes are somewhat irregular compared with those in DQSK, but no special significance could be associated with the irregular shapes. Grain size changes with heat treating conditions, but the ferrite fraction (not shown in the table) was relatively constant at about 0.95. Laboratory processing of the HSLA-V crop samples was not a valuable procedure to expand the range of microstructures to be evaluated beyond those of the mill samples.

The unknown factor in the microstructure is the state of vanadium precipitation; the aging experiments on mill-produced coil samples demonstrate the hardening potential from vanadium. The maximum strengthening from the 0.08 % vanadium addition can be estimated by comparing the DQSK coiled at 665 °C with the vanadium steel coiled at 690 °C and then aged at 600 °C for 1180 min; the grain size and ferrite fractions are nearly the same, but the strength of the aged vanadium samples were about 110 MPa higher than those for the DQSK coil. This value for precipitation strengthening is typical for a vanadium-containing steel, given the vanadium and nitrogen contents [16].

Table 8. Summary of all tensile tests on HSLA-V, 350 MPa grade steel.

Coil number and location[a]	Coiling temp., °C	Measured YS, MPa	Measured UTS, MPa	Grain size, mm
A1 – HR	—	356	464	—
A1[b] – HC	—	360	474	—
A1[b] – HL	—	343	453	—
A1[b] – MR	—	372	483	—
A1[b] – MC	692	377	493	8.5×10^{-3}
A1[b] – TR	—	360	474	—
A1[b] – TC	—	355	468	—
A1[b] – TL	—	350	465	—
A1[b] – TL	692	327	448	8.5×10^{-3}
A2[b] – MC	693	375	466	10.6×10^{-3}
A3[b] – MC	693	379	475	10.6×10^{-3}
A4 – HC	650	367	445	7.7×10^{-3}
A4 – TC	660	360	446	5.1×10^{-3}

Coil number and location[a,c]	Aging condition	Measured YS, MPa	Measured UTS, MPa	Grain size, mm
A1 – TL	600 °C/1180 min	430	504	—
Al – TL	720 °C /35 min	368–401	470	—
A1 – TL	720 °C /134 min	348–379	440	—
A1 – TL	720 °C /290 min	326	401	—
A1 – TL	720 °C /1200 min	231–264	333–357	—

[a] HR = head right; HC = head center; HL = head left; MR = middle right; MC = middle center; TR = tail right; TC = tail center; TL = tail left

[b] temper-rolled

[c] heat-treated at NIST

Figure 9. Typical microstructure for HSLA-V, 350 MPa grade. Bar in picture represents 10×10^{-3} mm.

4.3.1 Temper-Rolling

The YPE for the HSLA-V grade was distinctly different from that of the DQSK. The low values of YPE in the HSLA-V grade indicated that the samples had been temper-rolled after coiling. Temper-rolling can have some influence on the measured YS; usually, it decreases the YS. Temper-rolling has essentially no effect on UTS, so the net effect is an increase in the difference between YS and UTS. From table 8, the temper-rolled coil samples typically had a difference of 100 MPa to 115 MPa between YS and UTS, whereas the as-rolled coil samples showed a difference of 80 MPa to 85 MPa.

4.3.2 Within-Coil Variations

Samples from one HSLA-V coil were received in which nine separate areas in the coil could be studied and compared with each other to evaluate within-coil variations. The strengths varied with position in the coil, but the ferrite grain size and ferrite fraction did not. The data in table 9 show that there was a 50 MPa variation in YS and UTS depending upon the location within the coil. The maximum variation from sample to sample for identical material was about 10 MPa.

Table 9. Tensile test results from as-received HSLA-V coil A1.

Location	YP, MPa	LYS,[a] MPa	UTS, MPa	YP elong, %	Uniform elong, %	Total elong, %
Right edge	357	357	468	0.5	15	27
	356	356	460	0.7	16	31
Center	b	358	469	b	14	27
	b	367	479	b	16	28
Left edge	353	348	458	1.4	17	29
	337	337	448	0.6	17	28
Right edge	b	374	485	b	14	25
	369	369	482	0.6	16	29
Center	b	380	499	b	14	27
	b	375	486	b	13	25
Left edge	362	362	476	0.7	15	27
	363	358	472	0.9	16	28
Right edge	b	362	471	b	16	28
	b	349	465	b	16	28
Center	b	351	465	b	16	29
	b	350	465	b	15	29
Left edge	b	331	451	b	16	31
	b	324	445	b	18	34

[a] lower yield strength or offset yield strength, 0.2 %

[b] continuous yielding; no yield point

4.3.3 Influence of Test Orientation

The influence of test orientation on the hot-rolled coil samples was studied with the first HSLA-V coil. Samples from the head, middle, and tail where tested in the longitudinal (0°), transverse (90°), and diagonal (45°) orientations with respect to the rolling direction. The results summarized in table 10 indicate that the 0° orientation had the lowest YS, and the 90° samples had about 20 MPa higher strength; the strengths of samples from 45° were approximately the average of the other two.

Table 10. Summary of mechanical tests in HSLA-V steel as a function of orientation.

Coil and location	Strength, MPa			Elongation, %		
	YP	LYS	UTS	YP	Uniform	Total
Coil A4 – head						
long.	386	367	446	2.5	18.5	33
trans.	+25	+18	+5	+1.0	–0.5	–1
45°	+5	+13	+3	+0.4	–0.5	+2
Coil A4 – middle						
long.	377	370	455	1.5	16.5	31
trans.	+22	+16	–4	+1.0	—	0
45°	+27	+27	+16	+1.0	+0.5	+3
Coil A4 – tail						
long.	367	360	446	1.6	19.5	33
trans.	+31	+22	+5	+1.5	+1.5	–2.5
45°	+16	+13	0	+0.4	–0.5	–0.5
Coil A2 – middle						
long.	377	375	466	1.4	16.5	28.5
trans.	+17	+15	+8	+0.1	–1.5	–1.5
Coil A3 – middle						
long.	381	379	475	1.3	15	27.5
trans.	+14	+14	+1	+0.1	0	0

4.3.4 Aging of Coil Samples

A special set of tests was initiated to age the lowest-strength (most underaged) section of coil and to determine the properties as a function of the aging conditions. The results are summarized in table 11 for peak-aged and overaged conditions. With aging, the YPE returned to the typical values; the overall strength level peaked after 1160 min at 600 °C and then decreased with continued aging at 720 °C. The measured grain size of samples aged at 720 °C for 1200 min was the same as the that of the as-rolled samples; therefore, the increase in tensile properties was attributed to an increased volume fraction of precipitates, and the subsequent decrease was attributed to coarsening of precipitates. The peak strength occurred after aging at 600 °C for 1160 min. The UTS was similar to that of the sample taken from the middle section, center of width, but the YS of the peak-aged sample was about 50 MPa higher. We attributed the lower YS of the as-received coil to the temper-rolling.

Table 11. Tensile properties of aged coil samples, HSLA-V steel coil A1, left edge of tail section.

	Strength, MPa			Elongation, %		
ID	YP	LYS	UTS	YP	Uniform	Total
A-1	431	431	509	3.6	13.6	27
A-2	428	428	498	4.4	16.8	29.5
B-1	368	368	468	6.6	17.8	34
B-2	401	401	473	3.8	14.2	26
C-1	379	379	441	3.4	16	28
C-2	348	348	440	9.8	21	34
D-1	333	333	407	3.1	15.4	27
D-2	322	319	395	1.1	16.1	29
E-1	264	264	357	4.4	26	39
E-2	231	231	333	1.4	24.1	37

A = 600 °C/1160 min – peak-aged R_B 83
B = 720 °C/35 min – overaged R_B 78.2
C = 720 °C/134 min – overaged R_B 74.5
D = 720 °C/295 min – overaged R_B 69 to 72
E = 720 °C/1200 min – overaged R_B 63 to 66

4.4 HSLA-Nb, 350 MPa Grade Steel

A summary of all the tensile tests on these coil samples is shown in table 12. Tensile tests from laboratory-treated samples are summarized in table 13. Data for both as-received coil and heat-treated samples are included. The mechanical properties of the as-received samples were remarkably consistent: only a 24 MPa variation in YS and a 31 MPa variation in UTS. Laboratory processing of the HSLA-Nb crop samples was not a valuable procedure to expand the range of microstructures to be evaluated beyond those supplied from the mill. Figure 10 shows the microstructure that was typical of the HSLA-Nb; three orientations are shown in this case because they differed significantly. In the rolling plane, the alloy exhibited isolated patches of nonpolygonal grains with a higher second-phase content. In thicker products where toughness is important, these isolated patches could degrade the properties. The structure in the transverse view was used to correlate to longitudinal properties. The ferrite grain size for the four mill coils (shown in the table) varied from 3.6×10^{-3} mm to 4.7×10^{-3} mm, but the ferrite fraction (not shown in the table) was relatively constant at about 0.95. The grains were polygonal in nature, but not always equiaxed; the grain diameter was twice as large in the rolling direction. No correlation was found between the slight elongation of the grains and the mechanical properties that we are concerned with in this program.

Table 12. Summary for all tensile tests on HSLA-Nb, 350 MPa grade steel.

Coil number and location[a]	Coiling temp., °C	Measured YS, MPa	Measured UTS, MPa	Nb content, mass %	Grain size, mm
B1 – HC	662	461	529	0.041	4.2×10^{-3}
B1 – TC	650	460	528	0.041	4.1×10^{-3}
B1 – MC	666	472	541	0.035	4.7×10^{-3} (4.5×10^{-3})
B2 – HR	—	480	558	0.043	—
B3 – HC	—	482	555	0.043	—
B3 – HL	—	481	558	0.043	—
B3 – MR	—	473	558	0.043	—
B3 – MC	577	474	551	0.043	3.6×10^{-3} (4.0×10^{-3})
B3 – ML	—	477	552	0.043	—
B3 – TR	—	484	558	0.043	—
B3 – TC	—	470	549	0.043	—
B3 – TR	—	467	550	0.043	—
underaged – TC	—	466	527	0.036	3.7×10^{-3}

[a] HC = head center; HL = head left; HR = head right; MC = middle center; ML = middle left; MR = middle right; TC = tail center; TL = tail left; TR = tail right.

Table 13. Summary of all laboratory-treated HSLA-Nb steel samples.

ID[a]	Aging condition	Measured YS, MPa	Measured UTS, MPa	Nb content, mass percent	Grain size, mm
B3	750 °C/63 min	422	474	0.043	4.8×10^{-3}
B3	750 °C/76 min	405	466	0.043	4.9×10^{-3}
B3	650 °C/4290 min	465	516	0.043	4.9×10^{-3}
B3	750 °C/234 min	386	434	0.043	5.1×10^{-3}
B3	750 °C/234 min	343	417	0.043	5.4×10^{-3}
B3	700 °C/1400 min	439	472	0.043	4.9×10^{-3}
B3	600 °C/70 min	494	563	0.043	4.0×10^{-3}
underaged – TC	600 °C/100 min	494	552	0.036	3.7×10^{-3}
underaged – TC	550 °C/30 min	455	520	0.036	3.7×10^{-3}
underaged – TC	600 °C/210 min	490	552	0.036	3.7×10^{-3}
X – rolling – 1	as-received	391	471	0.041	5.4×10^{-3}
X – rolling – 2	as-received	433	—	0.041	8.9×10^{-3}
X – rolling – 2	600 °C/30 min	421	506	—	8.9×10^{-3}
X – rolling – 2	600 °C/100 min	438	523	0.041	8.9×10^{-3}
X – rolling – 2	525 °C/30 min	473	540	0.041	8.9×10^{-3}
X – rolling – 3	as-received	391	454	0.041	7.3×10^{-3}
X – rolling – 4	as-received	401	468	0.041	7.5×10^{-3}
X – rolling – 5	as-received	442	501	0.041	6.8×10^{-3}
X – rolling – 5	600 °C/30 min	445	514	0.041	6.8×10^{-3}
X – rolling – 5	600 °C/100 min	448	519	0.041	6.8×10^{-3}
X – rolling – 5	525 °C/30 min	455	520	0.041	6.8×10^{-3}
X – rolling – 6	as-received	399	469	0.041	8.1×10^{-3}

[a] TC = tail center; X indicates that the hot-rolling was done on an experimental mill

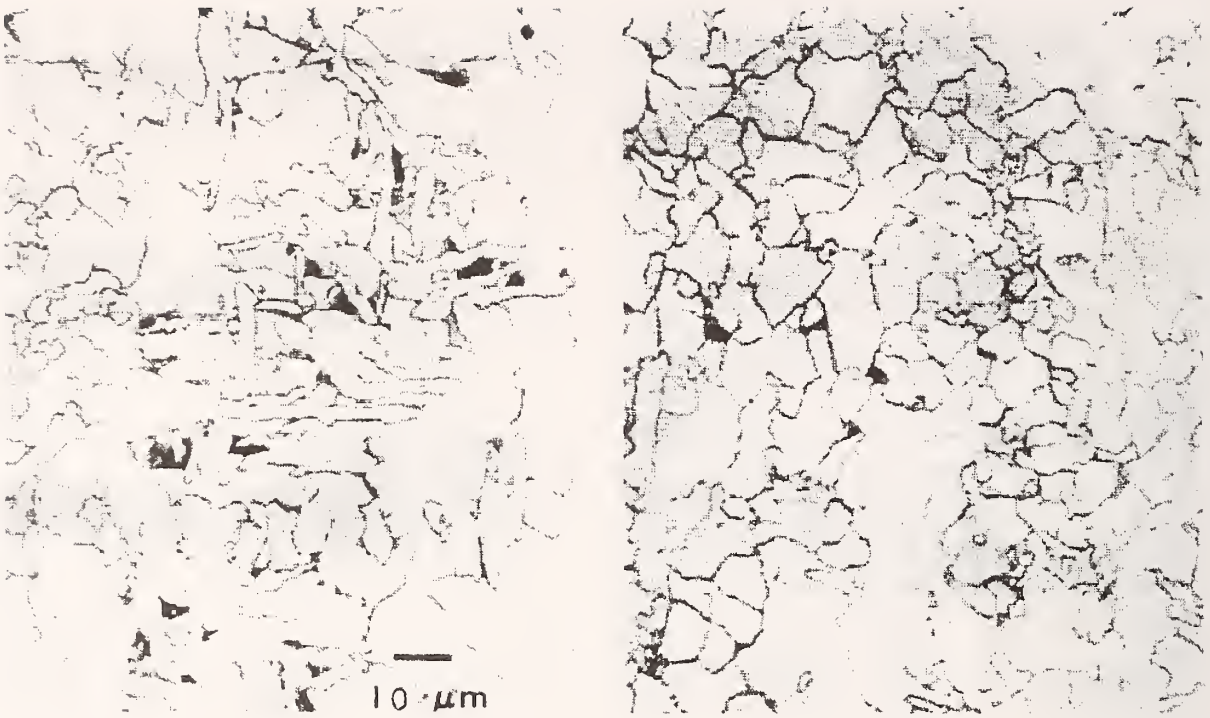

(a) (b)

(c)

Figure 10. Typical microstructure for the HSLA-Nb, 350 MPa grade steel: (a) rolling plane, (b) longitudinal, (c) transverse orientations. Bar in (a) represents 10×10^{-3} mm.

4.4.1 Within-Coil Variations

Samples from one HSLA-Nb coil were received in which nine separate areas in the coil could be studied and compared with each other to evaluate within-coil variations. The properties and microstructure varied little with position in the coil. Data in table 14 show that there was a 24 MPa variation in YS depending upon the location within the coil.

Table 14. Within-coil variations in tensile properties of HSLA-Nb coil B3.

Location	YP, MPa	LYS,[a] MPa	UTS, MPa	YP elong., %	Uniform elong., %	Total elong., %
Head						
right edge	488	476	557	—	—	23
	493	484	560	—	—	25
center	483	480	549	3.6	16	26
	501	484	561	3.5	15	26
left edge	490	481	558	3.2	16	24
	491	482	558	3.1	15	24
Middle						
right edge	494	473	558	3.2	16	26
	488	474	559	2.8	16	24
center–	486	474	549	3.6	16	26
long.	477	475	553	3.6	15	24
center–	522	517	577	4.3	16	26
trans.	516	511	571	3.9	15	24
left edge	489	472	549	3.5	16	24
	488	482	556	3.5	17	28
Tail						
right edge	493	488	557	3.3	16	25
	492	480	559	3.2	17	29
center	487	473	551	3.2	17	27
	482	468	547	3.4	14	22
left edge	475	469	550	2.8	16	24
	478	466	550	2.8	16	26

[a] LYS = lower yield strength or offset yield strength, 0.2 %

4.4.2 Aging of Coil Samples

Extra tests were initiated to determine the properties as a function of the aging conditions. Those results are summarized in table 15.

Table 15. Tensile test results from niobium steel after aging (heat-treated at NIST).

Sample	Strength, MPa			Elongation, %		
	YP	LYS	UTS	YP	Uniform	Total
HSLA–0.036 % Nb, extreme coil sample						
as-received, R_B 82, underaged, 3.7×10^{-3} mm grain size	466	466	528	3.8	15.7	27.1
	465	465	527	3.8	16.4	30.1
	466	466	525	3.5	15.6	29.0
	467	467	529	3.6	15.6	28.3
as-received + 550 °C, 30 min– R_B 81.5, underaged	456	453	518	3.6	17.0	26.9
	456	459	521	3.6	16.0	27.4
as-received + 600 °C, 100 min– R_B 87.5, peak aged	493	493	549	3.8	15.7	25.7
	495	495	554	3.8	15.3	25.2
as-received + 600 °C, 210 min– R_B 87.5, peak aged	481	487	549	3.8	15.6	27.7
	491	494	556	3.9	13.5	24.7
Coil B3 – Nb middle section						
as-received–R_B 87, underaged, 4.0×10^{-3} mm grain size		465–485	550–560	—	—	22–29
600 °C /70 min–R_B 87.4, peak aged, 4.0×10^{-3} mm grain size	511	494	566	3.9	16.4	26.5
	515	494	559	3.0	12.9	22.0
650 °C /4290 min– R_B 84.0, overaged, 4.9×10^{-3} mm grain size	498	463	516	5.4	15.4	25.5
	489	468	516	5.5	16.7	26.9
700 °C/1400 min– R_B 82.0, overaged, 4.9×10^{-3} mm grain size	464	438	472	6.5	17.2	27.9
	457	439	472	7.7	16.2	26.9
750 °C/63 min–R_B 78.6, overaged, 4.8×10^{-3} mm grain size	435	421	473	5.5	17.5	28.3
	454	424	474	5.5	16.1	25.2
750 °C/76 min–R_B 75.8, overaged, 4.9×10^{-3} mm grain size	434	413	467	6.3	16.1	25.7
	411	398	466	3.9	16.2	24.9
750 °C/234 min–R_B 71, overaged, 5.2×10^{-3} mm grain size	407	386	434	7.1	20.5	33.1
	358	343	417	4.9	19.7	30.1

4.5 HSLA-Nb–Ti, 360 MPa Grade Steel without Excess Titanium

A summary of the tensile tests for HSLA-Nb–Ti, 360 MPa grade steel without excess titanium) is shown in table 16. Only as-received coil samples are included. The mechanical properties of the as-received samples from the head and tail sections were remarkably consistent: 15 MPa variation in YS and 33 MPa variation in UTS. The typical microstructure observed in the HSLA-Nb–Ti, 360 MPa grade is shown in figure 11. The grains were polygonal, and little second phase was present. The ferrite grain size for the two coils (shown in the table) varied from 4.2×10^{-3} mm to 5.4×10^{-3} mm; the ferrite fraction was assumed to be 0.95.

Table 16. Summary of all tensile tests on HSLA-Nb–Ti, 360 MPa grade steel.

Coil number	Location[a]	Coil temp., °C	EQAD, mm	YS, MPa	UTS, MPa
C1	HC	644	4.2×10^{-3}	420	493
C1	TC	644	—	422	494
C2	HC	627	5.4×10^{-3}	414	507
C2	TC	627	—	417	502

[a] HC = head center; TC = tail center

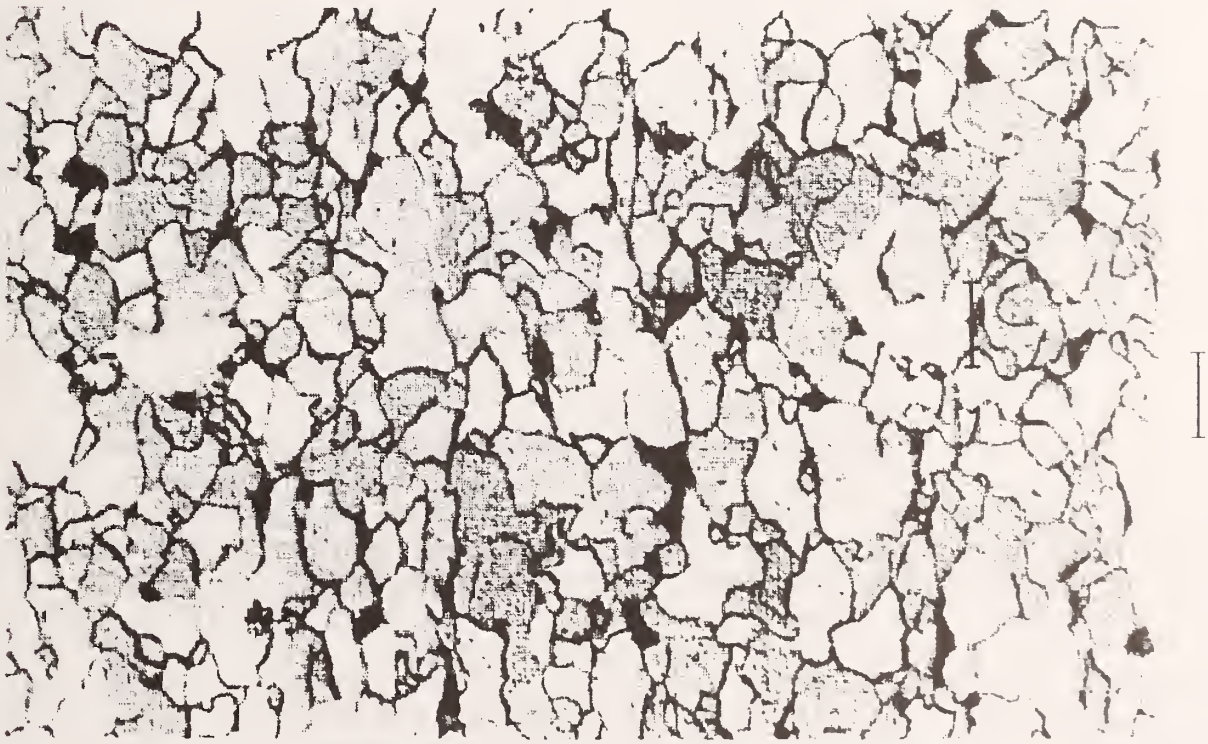

Figure 11. Typical microstructure for HSLA Nb–Ti, 360 MPa grade steel. Bar on the right represents 10×10^{-3} mm.

4.5.1 Within-Coil Variations

We received head and tail sections from two different coils (no middle section was included as was the case for the vanadium and HSLA-Nb–Ti steels); each section included a sample from the left edge, center, and right edge of the coil for a total of six different areas on each of two coils. The properties were extremely uniform, as mentioned earlier; the microstructure was not as uniform as that observed in the niobium grade, having a slightly larger distribution of grain sizes, but the variations are considered to be of little consequence.

4.5.2 Aging of Coil Samples

Only hardness tests were done on the aged coil samples. The hardness of the starting block for the aging experiment varied from R_B 78 to 81; this variation probably reflects the variations observed in the grain size and is important only on a local scale, as the tensile properties, which better reflect the bulk, were uniform. With aging at 650 °C, the hardness did not increase above 81, and it started to decrease after about 200 min.

4.6 HSLA-Nb–Ti, 550 MPa Grade Steel with Excess Titanium

A summary of the tensile tests for HSLA-Nb–Ti, 550 MPa grade with excess titanium is shown in table 17. As-received and heat-treated coil samples are included. Laboratory processing of the crop samples was not a valuable procedure to expand the range of microstructures to be evaluated beyond the as-received conditions.

The microstructure for the three coils of HSLA-Nb–Ti, 550 MPa grade are shown in figure 12. The grains were finer than in the lower-strength grades, and the morphologies were not always polygonal or equiaxed, which made the characterization of the structure difficult. The sample preparation for this grade was crucial. We did some color etching, and it tended to define the grain boundaries better for visual comparisons. After repeated examinations with both the light microscope and scanning electron microscope (SEM) and with a variety of etchants, there was no clear advantage for either technique in quantifying the grain size.

4.6.1 Grain-Size Measurements

Coil D2 that included head, middle, and tail sections was used for an interlaboratory comparison between UBC and NIST for grain-size measurements. One half of the broken, longitudinal tensile sample from the three positions (center location) was distributed to each laboratory. The undeformed grip area was sectioned, polished, and etched according to the usual procedure in each laboratory and examined in both the light microscope and SEM. The measurements for the grain sizes in the two laboratories are included in table 17; the measurements from UBC are listed first; those from NIST are in parentheses. For the head and tail center locations, there was excellent agreement: in the middle center location, staff at NIST measured a larger grain size (4.2×10^{-3} mm) than that measured at UBC (3.4×10^{-3} mm). This 0.8×10^{-3} mm difference in ferrite grain size amounts to about 30 MPa difference in the predicted strength, depending upon which equation is used. The grain-size sensitivity of the strength prediction is a concern for this high-strength grade in which the typical grain size is neither equiaxed nor polygonal.

Table 17. Summary of tensile tests on HSLA-Nb–Ti, 550 MPa grade steel.

Coil number and condition	Location[a]	Coiling temp.,°C or aging condition	EQAD, mm	YS, MPa	UTS, MPa	Remarks
D1						
as received	HC	648	2.9×10^{-3}	626	703	peak aged
as received	TC	642	2.9×10^{-3}	595	675	underaged
D2						
as received	HC	644	3.1×10^{-3} (3.3×10^{-3})	650	734	peak aged
as received	HL	644	—	633	703	peak aged
as received	MC	644	3.4×10^{-3} (4.2×10^{-3})	648	720	peak aged
as received	ML	644	—	645	722	peak aged
as received	TC	644	3.4×10^{-3} (3.6×10^{-3})	640	730	peak aged
as received	TL	644	—	635	724	peak aged
D3						
as received	TL	612	2.0×10^{-3} (2.9×10^{-3})	587	644	underaged
as received	MC	612	2.6×10^{-3} (3.2×10^{-3})	590	655	peak aged
aged	TL	525 °C/30 min	—	605	658	underaged
aged	TL	650 °C/10 min	—	608	658	underaged
aged	TL	650 °C/90 min	—	632	671	peak aged
D2[c]						
950 °C/60 min		air-cooled from 950°C	5.5×10^{-3}	372	459	b
950 °C/60 min		air-cooled from 790 °C	5.3×10^{-3}	349	449	b
950 °C/60 min		air-cooled from 650 °C	6.8×10^{-3}	328	431	b
950 °C/10 min		1°C/min cooling	—	333	423	b

[a] HC = head center; TC = tail center; HL = head left; MC = middle center; ML = middle left; TL = tail left

[b] no precipitation strengthening, low reheat temperature did not dissolve niobium in austenite

[c] heat-treated at NIST

4.6.2 Coil-to-Coil Variation

The differences in mechanical properties and microstructures for the three coils are shown in table 17 and in figure 12. The third coil with the lowest strength had the finest measured grain size. The chemical compositions reported for the three coils are very similar and cannot explain the variations in properties.

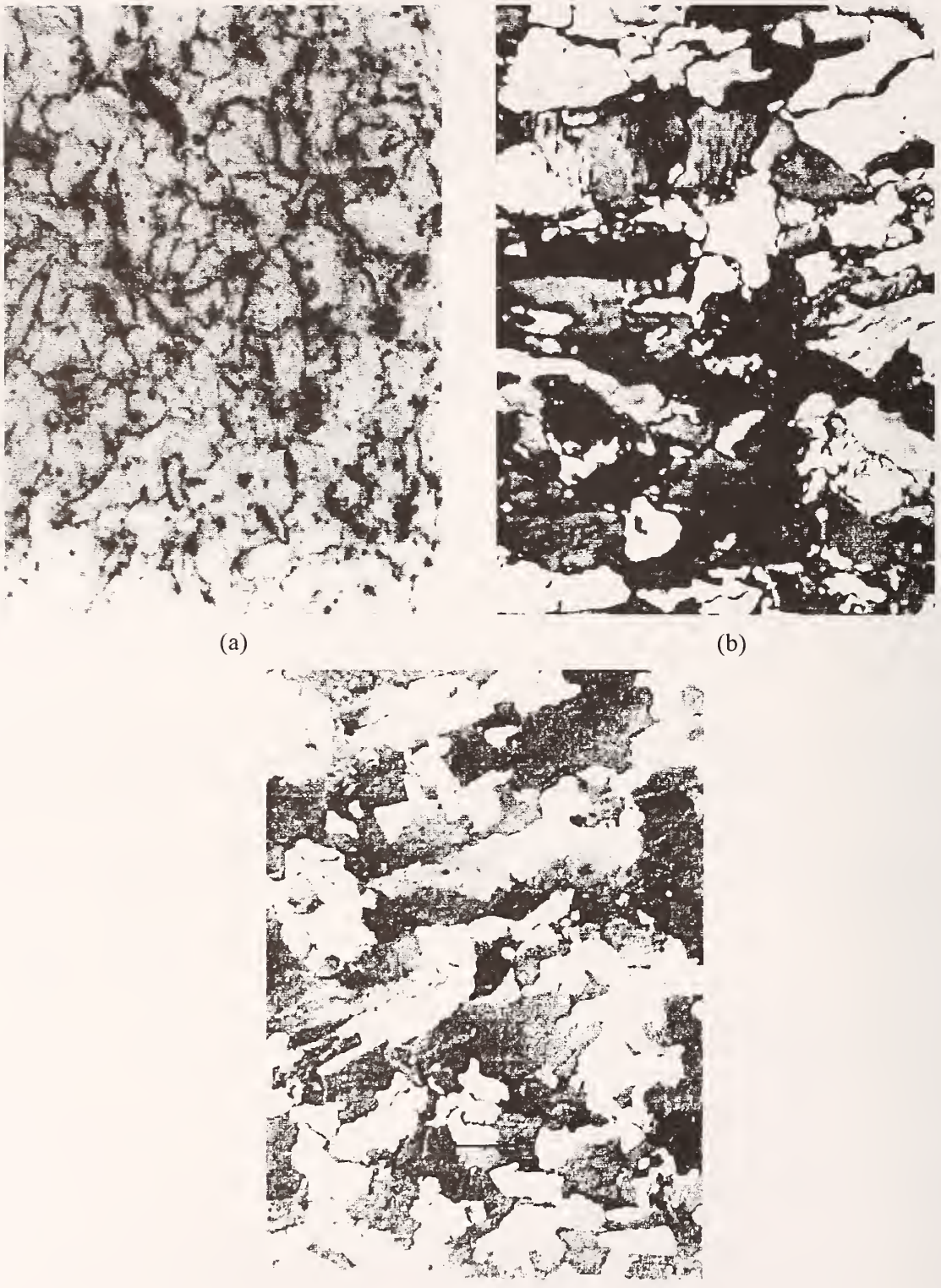

Figure 12. Microstructure for HSLA-Nb–Ti , 550 MPa grade steel. (1) coil D1, nital etchant, (b) coil D2, color etchant, and (c) coil D3, color etchant. Bar represents 5×10^{-3} mm.

4.6.3 Within-Coil Variations

The tail section from coil D1 had a lower strength than that of the head (about a 30 MPa difference). Coil D2 was checked in six locations, and the largest variations in strength were seen in the head section where the YS variation was 17 MPa and the UTS variation was 31 MPa. The as-received tensile properties of coil D3 were similar in the extreme tail and in the middle sections.

4.6.4 Aging of Coil Samples

Both hardness and tensile tests were done on aged coil samples. The tail section from coil D1 was aged at 650 °C for up to 1000 min and at 550 °C for up to 10 000 min; the results are shown in figure 13. At both temperatures, the peak hardness was the same, and the time it took to reach peak hardness was consistent with literature values for niobium steel [18].

Coil D2 increased in hardness less than three Rockwell points (B scale) with aging. Since no significance could be attached to this increase, no further experiments were performed on this material.

The middle section of coil D3 showed no increase in hardness with aging; the extreme tail section exhibited some aging response in the hardness test. Therefore, additional tensile samples from the extreme tail were machined and aged. The results of these tests are shown in table 18. The LYS increased about 40 MPa and the UTS was 30 MPa higher after 90 min at 650 °C. The relative change in strength was consistent with the increase in hardness observed in coil D2 after aging. These changes with aging reflect the relative importance of location within the coil on the strength.

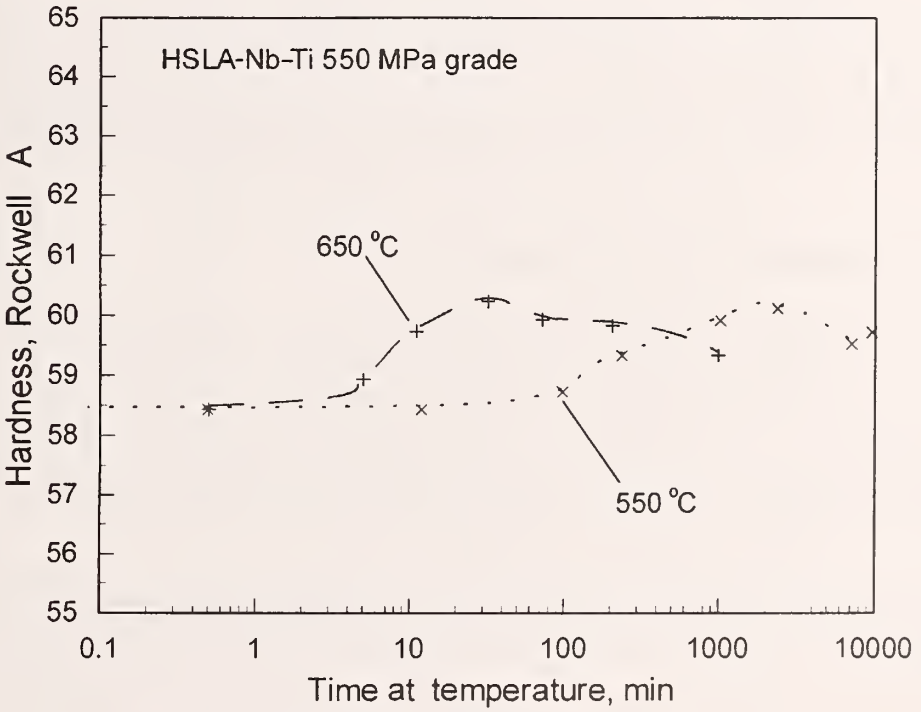

Figure 13. Hardness as a function of aging time for the HSLA-Nb–Ti, 550 MPa grade steel.

Table 18. Tensile test results from aged samples of coil D3, extreme tail section.

Condition and sample number	YP, MPa	LYS, MPa	UTS, MPa	YP elong., %	Uniform elong., %	Total elong., %
As received						
1	583	583	650	2.6	10.6	19.4
2	594	591	637	3.1	12.0	22.8
525 °C for 30 min						
1	608	606	666	2.6	10.4	19.4
2	608	604	651	3.9	12.0	21.8
650 °C for 10 min						
1	642	610	659	3.4	11.1	20.0
2	636	606	657	3.6	11.8	20.9
650 °C for 90 min						
1	650	630	669	4.1	10.8	19.0
2	656	635	673	3.6	10.6	20.0

4.6.5 Effect of Heat Treatment

Additional tests were performed on the HSLA-Nb–Ti, 550 MPa grade steel to confirm that, after processing, its grain size was coarser and the effects of precipitation were gone. The heat treatment took as-received sheets and reheated the material to 950 °C for 1 h and then cooled it at different rates. The low reheat temperature of 950 °C ensures that little niobium and titanium will be dissolved in the austenite and that they will be available for subsequent precipitation in ferrite. The results are summarized in table 17.

4.7 Nb–Ti and Niobium-Lean IF Grade Steel

The work on this grade for the structure–properties subtask was limited because no IF grade steel is sold after hot-rolling. A summary of the tensile tests is shown in table 19. Only as-received coil samples are included. The microstructures for the IF sheets were coarser than those of any of the other grades included in the program, and the microstructures revealed some differences in grain size and shapes. Grain shape is not considered to have a significant effect on the properties. The variation in the LYS for the tail sections indicated that processing had some effect, but the UTS showed little effect, and we concluded that the influence of processing is small and can be neglected.

The microstructure typically observed in the Nb–Ti and titanium IF grade is shown in figure 14. The second phase observed in the other grades was absent because there was essentially no carbon in these steel grades.

Table 19. Tensile test results from the IF steel coils.

Coil and location	YP, MPa	LYS, MPa	UTS, MPa	YP elong., %	Uniform elong., %	Total elong., %
Nb–Ti, E1	272	260	332	3.6	26.0	45
tail center	276	259	330	3.3	24.6	43
Nb–Ti, E2	261	251	329	3.5	25.4	42
head center	260	249	327	3.3	25.2	43
	253	244	329	3.3	23.8	47
	255	246	330	2.2	23.0	45
Nb–Ti, E2	296	296	334	3.3	21.9	42
tail center	292	281	333	3.3	21.4	40
	283	265	333	3.6	22.4	41
	263	249	327	3.3	25.5	45
Nb–Ti, E3	258	255	330	3.0	21.7	38
head center	259	248	327	2.7	22.4	38
	258	253	332	2.4	21.4	40
	262	254	333	2.4	22.4	41
Nb-lean, E4	237	231	310	3.3	23.6	41
head –	232	231	312	3.6	23.9	38
longitudinal	230	226	312	3.3	22.5	44
	225	225	308	2.7	23.6	40
tail –	273	258	316	4.1	22.8	41
longitudinal	291	280	308	3.5	20.8	41
	261	250	307	3.8	27.9	44
	262	255	317	4.6	25.0	45
Nb-lean, E5	230	220	311	2.8	23.9	45
head – longitudinal	227	217	301	2.4	24.3	45
tail –	264	256	316	3.3	23.0	45
longitudinal	267	258	323	3.6	22.8	45
head –	276	256	303	5.4	24.3	45
transverse	284	266	319	3.6	22.7	43
tail –	282	263	320	5.4	22.8	46
transverse	295	271	321	5.7	23.0	45

(a)

(b)

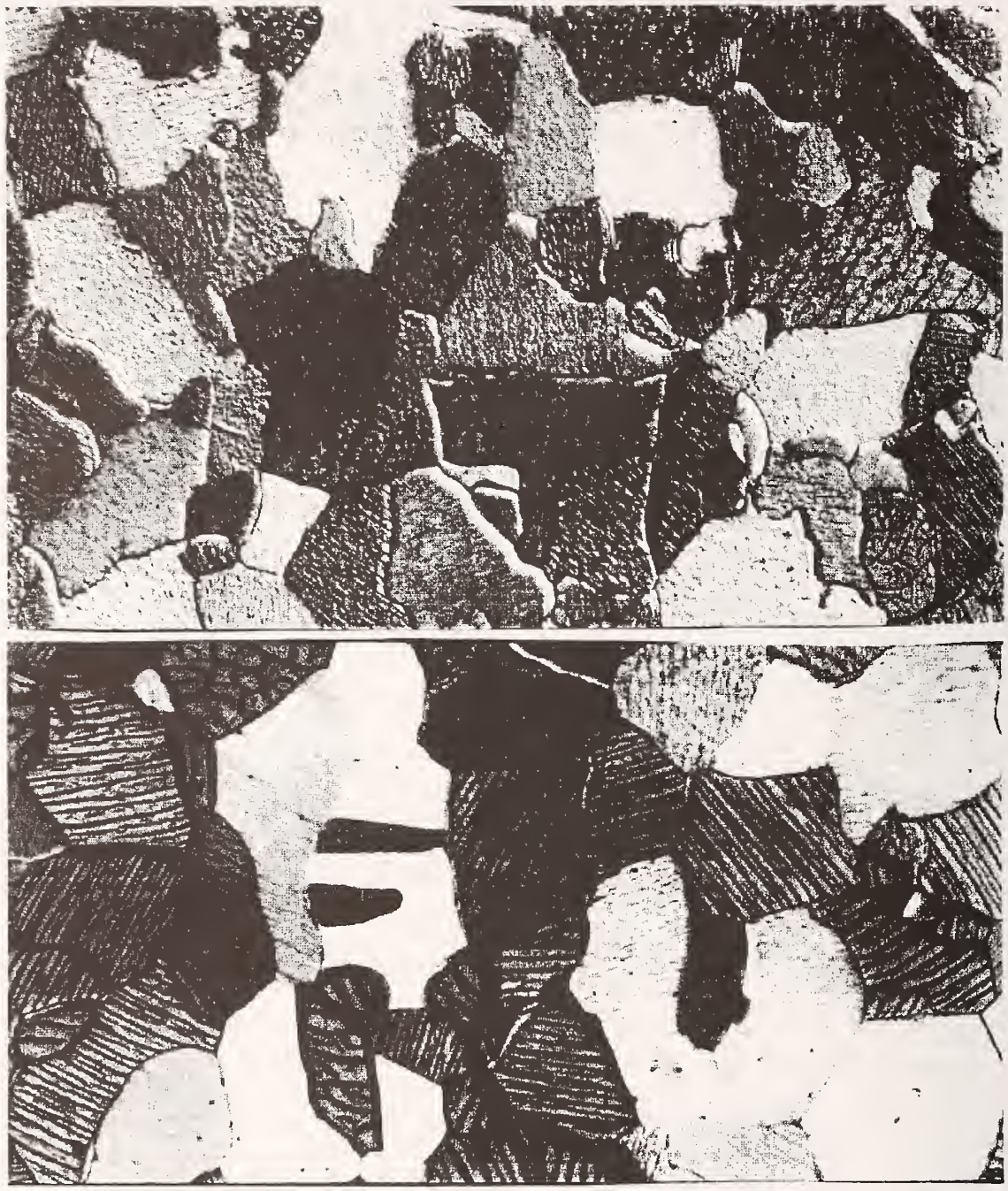

Figure 14. Typical microstructure observed in the (a) Nb–Ti and (b) Ti IF steel grades. Bar respresents 10×10^{-3} mm.

4.8 Other HSLA-Nb Grade Steel

Samples from other HSLA-Nb grades (0.06 % carbon, 0.7 % manganese, 0.02 % to 0.03 % niobium) were collected from three companies to supplement the data base available for the development of property predictions. The coils from one company had been temper-rolled; the others, as-rolled. All the chemical compositions were similar, but each had a different mill setup. The tensile test results are summarized in table 20. A check of the microstructure revealed consistently polygonal and nearly equiaxed grains. The temper-rolled samples (with different thicknesses) showed the effects of increasing hot deformation: refining the austenite grain size reduced the final ferrite grain size (see fig. 15). Figure 16 shows the material's microstructure as well as the effects of color and nital etchants in preparing the sample. Figure 17 shows the microstructure from onesample, which, again, was very similar to those found in the other HSLA-Nb samples from other companies.

Table 20. Summary of tensile tests for HSLA-Nb coils from different mills.

Coil number and location[a]	Coiling temp., °C or aging condition	EQAD, mm	YS, MPa	UTS, MPa
F1 – TC	678	4.9×10^{-3} (5.3×10^{-3})	436	509
F2[b] – HC	675	4.4×10^{-3}	422	533
F2[b] – TC	675	3.9×10^{-3}	418	527
F2 – TC	600 °C/100 min	3.9×10^{-3}	469	530
F3[b] – HC	675	4.2×10^{-3}	408	505
F3[b] – TC	675	5.0×10^{-3}	405	495
F4[b] – HC	550	4.8×10^{-3}	427	525
F4[b] – TC	550	4.4×10^{-3}	423	530
F5[b] – HC	550	4.7×10^{-3}	426	527
F5[b] – TC	550	4.6×10^{-3}	428	535
F5 – TC	600 °C/100 min	4.6×10^{-3}	481	545
F6[b] – HC	600	5.9×10^{-3}	405	512
F6[b] – TC	600	5.6×10^{-3}	406	515
F6 – TC	600 °C/100 min	5.6×10^{-3}	431	488
F7[b] – HC	600	6.0×10^{-3}	405	510
F7[b] – TC	600	5.0×10^{-3}	393	515
F8 – MC	655	5.2×10^{-3}	386	468

[a] TC = tail center; HC = head center; MC = middle center

[b] temper-rolled

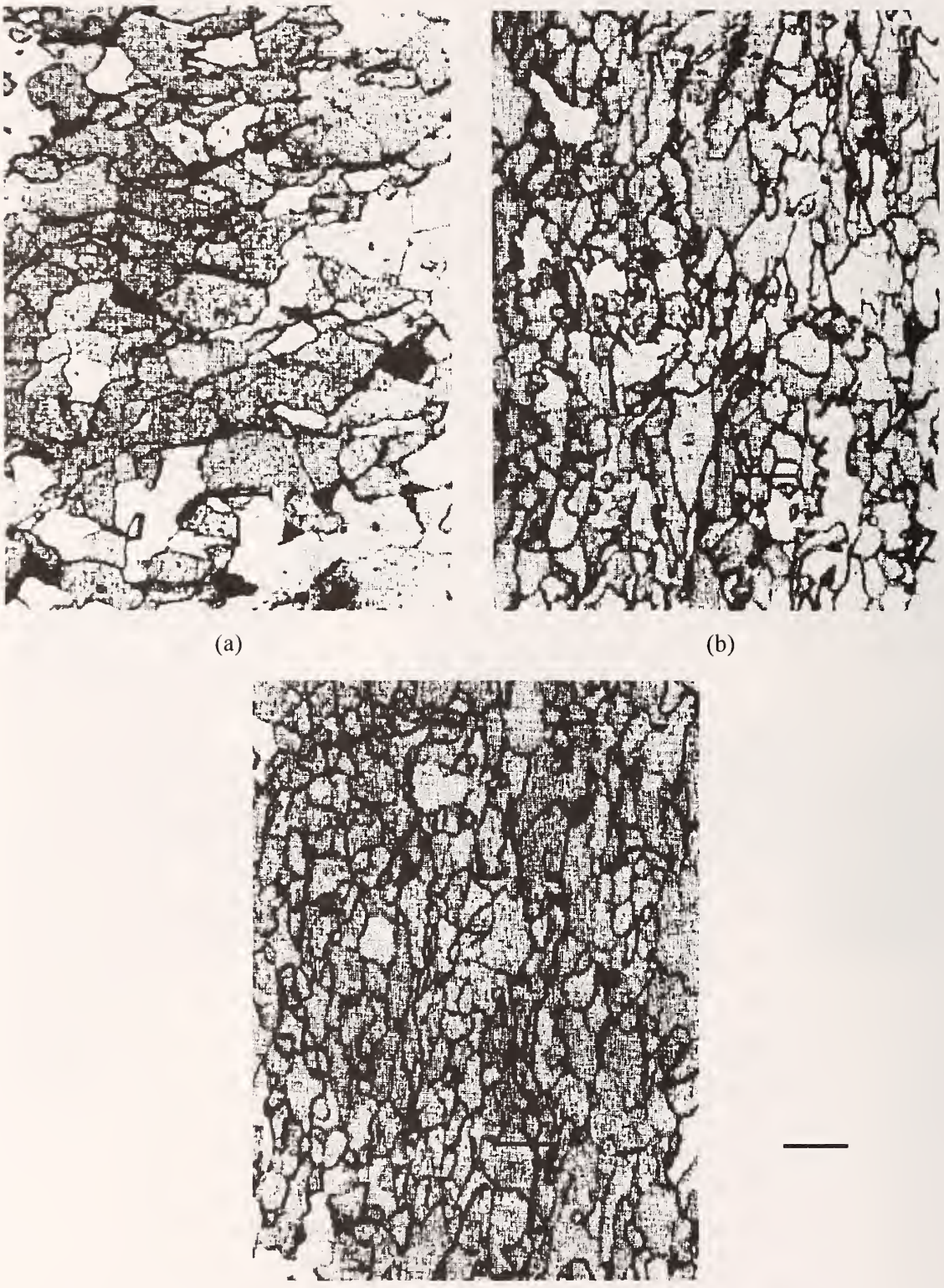

Figure 15. Microstructure for the HSLA-Nb, 350 MPa steel with different thicknesses: (a) 6 mm, (b) 4 mm, and (c) 1.8 mm. Bar represents 10×10^{-3} mm.

(a)

(b)

Figure 16. HSLA-Nb coil microstructure: (a) nital etchant and (b) color etchant. Bar in picture represents 20 $\times 10^{-3}$ mm.

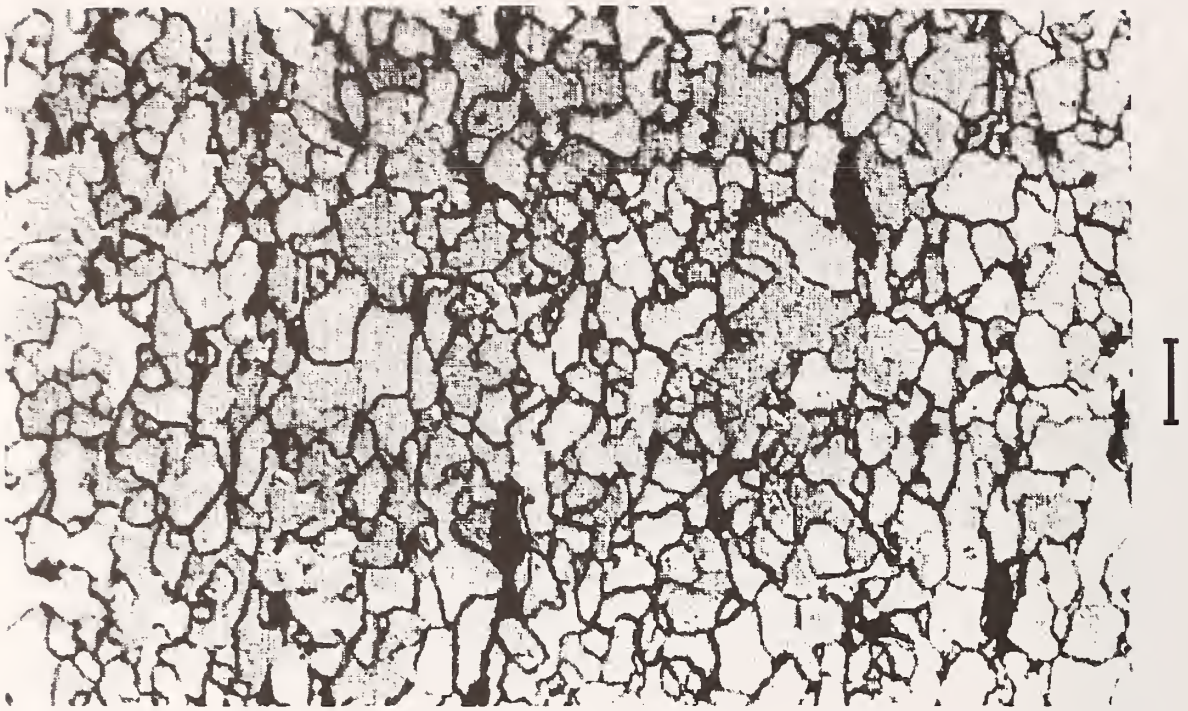

Figure 17. Typical microstructure for HSLA-Nb, 350 MPa grade steel, coil F8. Bar represents 10 $\times 10^{-3}$ mm.

4.8.1 Within-Coil Variations

We received samples from nine locations for coil F8; head, middle, and tail sections were included that spanned the full width of the coil. The results of the tensile tests are shown in table 21. The largest variation in the LYS was 21 MPa: the UTS variation was 19 MPa. The samples from other steel companies did not allow for a significant comparison of within-coil variations.

4.8.2 Aging of Coil Samples

Both hardness and tensile tests were done on aged coil samples from coils F2, F5, and F6. The as-received coils were aged at 600 °C for 100 min. Each showed some increase in hardness with aging, between 2 and 3 points Rockwell B. To document the corresponding change in tensile properties, the aging was repeated on samples large enough for tensile testing from three of the coils with different thickness and coiling temperatures. The results are shown in table 22. In each case, the LYS increased with aging, from 26 MPa to 54 MPa; the biggest increase was for the sheet coiled at 550 °C. For the UTS, only the sheet coiled at 550 °C exhibited an increase; the UTS for the sheet coiled at 600 °C actually decreased by 26 MPa. The temper-rolled condition of the as-received coils could account for at least a 20 MPa to 30 MPa difference in the LYS and no change in the UTS. In conclusion, it appears that the sheets coiled at temperatures above 550 °C were at their maximum strength possible, given the ferrite grain size produced on the runout table. For the sheet coiled at 550 °C, the low coiling temperature resulted in a slightly lower strength ($\leq$15 to 25 MPa) than possible.

Table 21. Tensile test results from coil F8.

Location	YP, MPa	LYS, MPa	UTS, MPa	YP elong., %	Uniform elong., %	Total elong., %
Head						
left	399	393	474	2.0	19.5	31.2
center	383	380	462	—	—	31.0
right	380	375	460	1.9	18.9	30.7
Middle						
left	404	401	474	3.3	19.2	30.4
center	392	386	468	2.7	18.6	31.0
right	398	395	467	3.1	20.3	31.0
Tail						
left	400	387	455	4.1	19.7	30.4
center	403	397	455	4.7	21.4	34.0
right	398	392	456	3.3	19.2	31.0

Table 22. Tensile test results from niobium-treated coils F2, F5, and F6.

Coil number and description	YP, MPa	LYS, MPa	UTS, MPa	YP, %	Uniform elong., %	Total elong., %
Coil F2 – 1.9 mm thick; 675 °C coiling; as-received; 600 °C/100 min	420	420	530	1.0	16	24.5
	475	469	530	5.0	19.5	28.5
Coil F5 – 4.0 mm thick, 550 °C coiling; as-received; 600 °C/100 min	430	427	530	0.8	17.0	28
	498	481	545	3.4	16.0	27.5
Coil F6 – 6.2 mm thick, 600 °C coiling; as-received; 600 °C/100 min	405	405	514	0.8	17.5	31
	438	431	488	3.5	18.4	32.5

4.9 Ferrite Grain-Size Measurements—Round Robin

Because ferrite grain size is such a critical factor in the program, an interlaboratory round robin to evaluate the measurement of ferrite grain size was initiated between the sponsor companies, UBC, and NIST. UBC prepared five samples to be evaluated by each laboratory according to the procedures that they currently use; one of the samples was from an A36 coil (number 1) and the other four were from DQSK (number 2 was an actual coil sample; the other three were coil samples that were heat-treated to increase the grain size). The results are summarized in table 23.

The results emphasize that the measurement of grain size is not as precise as, for example, the measurement of mechanical properties like UTS. The grain size measurement typically averages

Table 23. Summary of ferrite grain size from round robin.[a]

ID	Method	Sample number				
		1	2	3	4	5
UBC	area	7.0×10^{-3}	10.0×10^{-3}	20.0×10^{-3}	25.0×10^{-3}	47.0×10^{-3}
NIST	intercept	7.0×10^{-3}	10.9×10^{-3}	22.8×10^{-3}	29.1×10^{-3}	69.7×10^{-3}
A	intercept	6.8×10^{-3}	10.3×10^{-3}	22.1×10^{-3}	26.2×10^{-3}	60.2×10^{-3}
B	intercept	8.9×10^{-3}	11.9×10^{-3}	26.5×10^{-3}	31.4×10^{-3}	74.2×10^{-3}
C	intercept	9.6×10^{-3}	11.9×10^{-3}	24.1×10^{-3}	27.6×10^{-3}	75.1×10^{-3}
D	area	12.5×10^{-3}	15.4×10^{-3}	25.3×10^{-3}	33.0×10^{-3}	76.5×10^{-3}
E	comparison	10.7×10^{-3}	15.1×10^{-3}	25.3×10^{-3}	35.8×10^{-3}	101.3×10^{-3}
F	area	7.5×10^{-3}	11.2×10^{-3}	b	27.1×10^{-3}	56.9×10^{-3}
G	area	5.1×10^{-3}	10.0×10^{-3}	b	29.6×10^{-3}	56.4×10^{-3}

[a] Values reported are EQAD in millimeters

[b] Not available; sample was repolished between measurements and fell out of the mount

500 grains in one cross section; a measured mechanical property like UTS is averaged over the entire test section that includes several orders of magnitude more grains in the cross section. The agreement in the measured values from UBC and NIST is important because there has to be consistency within the program. The program will output a ferrite grain size, but it is the comparison between the property measurement at each company and the computer prediction of the mechanical property that is the ultimate standard by which the program is judged. Users of the program will have to judge how the grain size output from the program is used in comparison with their own measured values.

5. Discussion

The discussion focuses on the two main contributions to strength: base strength (grain refinement and solid-solution strengthening) and precipitation.

5.1 Equations to Predict Properties

5.1.1 Plain-Carbon Steel: Base Strength

The approach taken for the two plain-carbon steel grades considered in the program is that only grain refinement and solid-solution strengthening contribute to strength in the as-rolled sheets produced in the hot-strip mill.

5.1.1.1 Review of Equations in the Literature

Five sets of equations found in the literature are relevant to the hot-strip mill model: the following equations from Pickering [2, 11], Hodgson and Gibbs [7], Choquet et al. (IRSID) [3], Tomota et al. [8], and Campbell et al. [12].

Pickering:

$$YS = 88 + 37[Mn] + 83[Si] + 2918[N_{free}] + 15.1d^{-1/2} \quad (3)$$

$$UTS = 294 + 28[Mn] + 83[Si] + 3.85[f_p] + 7.7d^{-1/2} \quad (4)$$

Hodgson and Gibbs:

$$YS = 62.2 + 26.1[Mn] + 60.2[Si] + 3286[N_{free}] + 19.7d^{-1/2} \quad (5)$$

$$UTS = 164.9 + 53.6[Mn] + 99.7[Si] + 634.7[C] + 11d^{-1/2} \quad (6)$$

Choquet et al. (IRSID):

$$YS = 63 + YS_{ss} + k_y f_\alpha d_\alpha^{-1/2} + (360 + 2600[C]^2)(1 - f_\alpha), \quad (7)$$

and

$$UTS = 237 + UTS_{ss} + k_t f_\alpha d_\alpha^{-1/2} + 500(1 - f_\alpha), \quad (8)$$

where

$$YS_{ss} = 23[Mn] + 53[Si] + 700[P] + 5000[N_{free}],$$

$$k_y = 15.4 - 30[C] + 6.094/(0.8 + [Mn]),$$

f_α = ferrite fraction,

d_α = ferrite grain size (in millimeters),

$$UTS_{ss} = 29[Mn] + 79[Si] + 700[P] + 5369[N_{free}],$$

$$k_t = 7.24.$$

Tomota et al.:

$$\sigma = a(b + \varepsilon_p)^N, \quad (9)$$

where

$$a = 373 + 62.7[Mn] + 109[Si] + 10.8d_\alpha^{-0.5},$$

$$b = 0.002,$$

$$N = 5.35/(10 + d^{-0.5}) - 0.024[Mn] - 0.037[Si] - 0.12$$

so that

$$YS = \sigma \text{ at } \varepsilon_p = 0.002 \quad (10)$$

and

$$UTS = a[N]^N. \quad (11)$$

Campbell et al.:

$$\mathrm{YS} = f_\alpha (132 + 11.8 d_\alpha^{-1/2}) + (1 - f_\alpha)(408 + 92.2[\mathrm{Mn}] + 0.400 S_P^{-1/2}) + 79.7[\mathrm{Si}] \quad (12)$$

$$\mathrm{UTS} = f_\alpha (197 + 15.9 d_\alpha^{-1/2}) + (1 - f_\alpha)(592 + 0.791 S_P^{-1/2}) + 500[\mathrm{Si}], \quad (13)$$

where

YS and UTS are in megapascals,
d is in millimeters,
elemental composition is in mass percent, and
S_P is the pearlite spacing in micrometers.

Tomota's equations are best applied to low-carbon steel with no appreciable free interstitial content; the YS cannot be considered for a typical hot-strip product where there is appreciable YPE. The equations from Campbell et al. require additional information about the pearlite spacing that is not predicted from the transformation model. For comparison purposes, we assumed the spacing to be 0.4 μm; serious considerations of these equations would require expansion of the transformation model to include interstitial solute content and pearlite spacing. We include them here because they could be used for future applications.

A consideration in choosing the equations to predict strength is the grain size dependence. Ferrite grain sizes of plain-carbon steel typically vary from about 6×10^{-3} mm to 20×10^{-3} mm. However, we used the equations developed from plain-carbon steel also for microalloyed steel to evaluate the precipitation-strengthening contribution. The ferrite grain sizes in microalloyed steel are typically finer than those observed in plain-carbon steel; a ferrite grain size as small as 2.5×10^{-3} mm has been observed in a Nb–Ti steel [18]. Therefore, the equations must work for the smaller grain sizes as well.

A different, but important issue relates to the way in which the second phase affects the strength. One approach for the prediction of YS, taken by Pickering and Hodgson and Gibbs, assumes that the properties of ferrite control the YS until the volume fraction of second phase reaches 20 %, which is sufficient for nearly all the conditions with which we are concerned. Campbell et al. and Choquet et al. took a different approach, assuming a simple rule-of-mixtures equation to predict the LYS, but over a wider range of f_α than that is applicable in the previous approach.

For UTS, each of the four equations deals with variations in f_α in a different fashion. The equation of Choquet et al. assumes the rule-of-mixtures with a constant strength for the pearlite; the equation from Campbell et al. has the same assumption, but with a dependence on pearlite spacing. Pickering limits the equation to less than 20 % second phase with a linear dependence of UTS on the perlite volume fraction f_P and not on composition or spacing. Hodgson and Gibbs assume the contribution of f_P depends on the carbon content and not on microstructural details, pearlite spacing, or volume fraction.

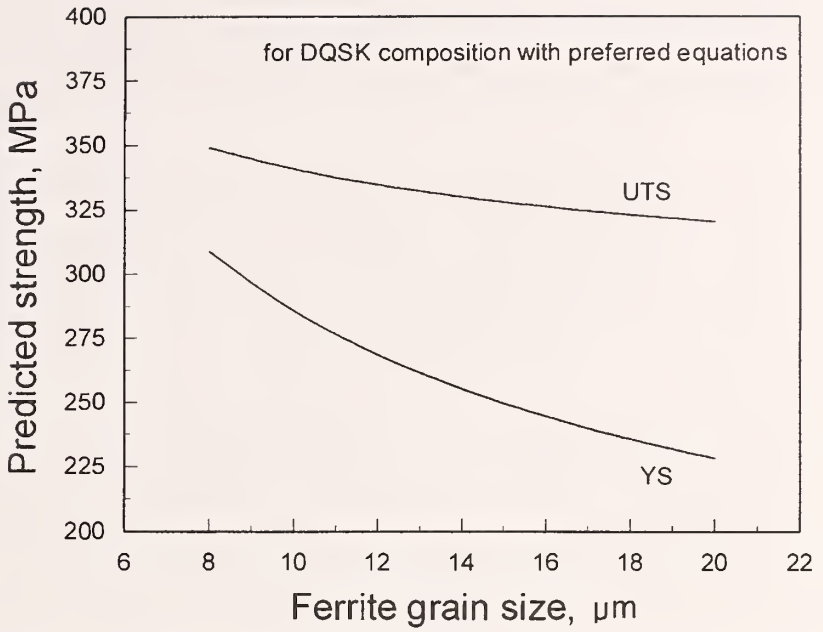

Figure 18. For DQSK, predicted YS and UTS from preferred set of equations as a function of grain size.

5.1.1.2 Application to the Hot-Strip Model

For the final hot-strip model released by UBC to AISI, the equations of Choquet et al. have been adopted to describe the base LYS and UTS for several reasons: (1) The equations were developed for a wider range of composition and f_α than we need and, therefore, they should be adequate for all cases. (2) Complication of the transformation model with the prediction of pearlite spacing is unnecessary. (3) The equations predict a reasonable behavior for grain sizes between 20 mm and 8 mm (see fig. 18), which is typical for plain-carbon steel.

An alternate set of equations to use for the prediction of strength in plain-carbon steel would be the YS equation from Pickering and the UTS equation from Hodgson and Gibbs. A major reason to use Pickering's YS and Hodgson and Gibbs's UTS equations together is that they give a consistent value for the contribution of precipitation in HSLA steel.

5.1.2 HSLA Steel: Precipitation Strengthening

Precipitation strengthening is the result of the interaction between dislocations and the carbonitrides containing vanadium, niobium, and/or titanium that form on cooling HSLA steel. The enhanced strength is a strong function of composition (volume fraction) and the distribution of particle size and spacing. Numerous approaches to predict the strengthening have been used; we review many of these in the following subsections and then recommend how to implement the prediction.

5.1.2.1 Review of Equations in the Literature

We have compiled a list of physically based equations found in the literature [5, 7, 17, 19–26] that relate to the strengthening increment due to precipitation; the proposed equations are shown in table 24. In most cases, the strengthening is calculated from structural parameters measured on carbon extraction

Table 24. Equations found in the literature to describe precipitation strengthening.

Source	Relationship
Gladman [19]	$(5.9 \times f^{1/2} x^{-1}) \ln (x/b)$
Melander [20]	$0.7\left[\frac{Gb}{\lambda}\right] \ln(\lambda/b) \ \ln\left[\frac{2d_g\lambda}{(d_g+\lambda)b}\right][\ln(\lambda/b)]^{-3/2}$
Martin [21]	$2Gb\lambda^{-1}$
Gawne and Lewis [22]	$(8.9 \times f^{1/2} \lambda^{-1}) \ln(1630x)$
Parilák et al. [23]	$38 + 76.8 \times 10^{-8}\lambda^{-2}$
Hodgson and Gibbs [7]	$2500 \times Nb_{sol}$
Mitchell et al. [5]	$(k_1 N_{eff} - k_2)V^{1/2}$
Österle [24]	$0.519\ Gb\lambda^{-1} \ln (x/b)$
Kwon et al. [25]	$kV_\alpha f^{1/2} x^{-1}$
NIST [26]*	$373[1 - \exp(-6.33Nb_{sol})]^{0.426}$
NIST [27]	kf_c

* Process dependent

f = volume fraction of precipitates, subscript c for calculated; otherwise measured from replica
b = Burgers vector, 0.25 nm
λ = interparticle spacing
x = average particle diameter
d_g = geometric mean-particle diameter from extraction replicas
V_α = volume fraction of ferrite
k, k_1, and k_2 = fitting parameters
N_{eff} = effective N content = (total N) – (1 % Ti)/3.42
assumes Poisson's ratio = 0.3

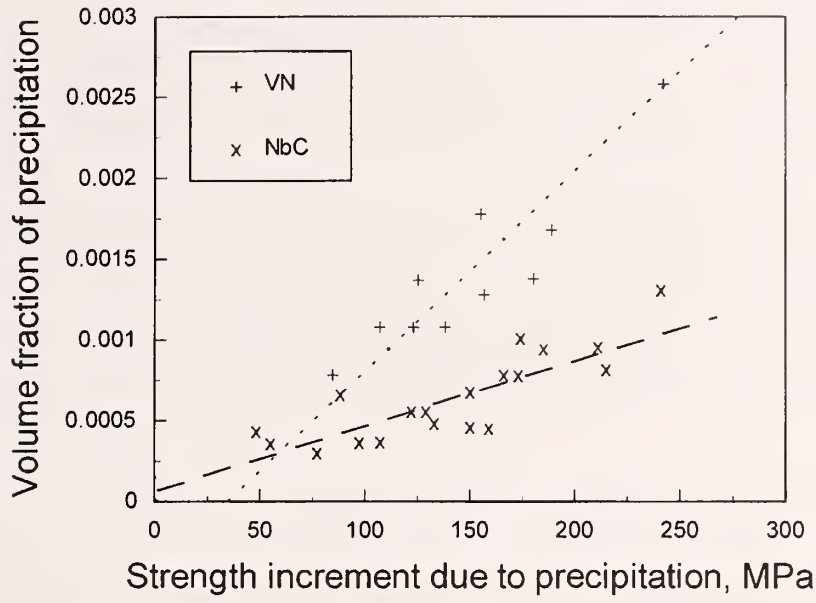

Figure 19. Calculated precipitation strengthening as a function of estimated volume fraction of particles for NbC [18] anc VN [28].

replicas like the particle size x, average particle spacing λ, and/or the particle volume fraction f. However, there is no consistency among the equations. Some equations assume that only the average particle spacing is important. Only Melander [20] takes into account the size distribution of particles. In other approaches, the concentration of the metal species (either vanadium or niobium) is taken as an estimate of the volume fraction f. The calculated f, based on the temperature history and chemical composition [26], can be correlated to strength as a linear function, as NIST has done for the case of continuous cooling, or taken as a function of the square root of the volume fraction estimated by Zajac et al. [28]. All these approaches have been shown in the literature to work for a given set of data. Two complications for the predictions that depend only on calculated f are (1) they cannot predict overaging (the case where the volume fraction is a maximum and the particle sizes are coarse) and (2) the strengthening from a given f of NbC is different from that of VN particles (see fig. 19).

A different approach to predicting variations in the precipitation strengthening in aluminum alloys has been proposed by Shercliff and Ashby [29]. Their process model takes into account the particle coarsening and changes to the solid-solution strengthening. The time constants for each process involved are combined, and the effective activation energy for the system is measured so that the kinetics of aging is characterized. This approach requires evaluating the kinetics through a series of experiments, but once the activation energy for a particular system is measured, the aging kinetics for any time–temperature history can be predicted.

5.1.2.2 Application to the Hot-Strip Model

For the hot-strip model, we used the Shercliff–Ashby model; its application is summarized in reference [29]; this approach eliminates the need to characterize in detail the particle size and spacing in HSLA steel. Such measurements are always time-consuming and subject to large experimental errors. The experiments required to implement the Shercliff–Ashby model are simpler to perform and are readily integrated into the hot-strip model. The main problem associated with the Shercliff–Ashby model is

obtaining suitably underaged material on which to perform the required experiments. For the HSLA-V grade, the head and tail sections from the as-received coils were acceptable. Aging experiments at different temperatures were performed, and the sample hardnesses are shown in figure 20. The time it takes to reach the peak hardness can be plotted against the aging temperature to calculate the effective activation energy Q; for the HSLA-V grade that value is 4 eV.

For the remaining HSLA (niobium-containing) steel grades, there is a fundamental problem to obtain material that is underaged. The as-received coil samples were within 3 Rockwell B points of the peak hardness that could be measured after aging experiments. In laboratory testing of crop samples, the samples were reheated to 1200 °C, furnace-cooled to 950 °C, thermomechanically processed to refine the austenite grain size, and then water-cooled. The resulting microstructures contained at least 50 % non-polygonal constituents, and only a 3-point Rockwell B increase was found after aging the samples to the peak hardness.

A paper by Vollrath et al. [17] contained aging curves performed on a 0.09 % carbon, 0.72 % manganese sheet steel with 0.046 % niobium that had been coiled at low temperatures to suppress precipitation during coiling (490 °C to 540 °C). The aging kinetics in Vollrath's work was similar to that found in our aging experiments on as-received coil samples and the laboratory-processed crop samples of niobium steel. Figure 21 compares the aging curves for one of the laboratory-processed crop samples and one reported by Vollrath [17]. The absolute strengths were quite different, but the kinetics of precipitation appeared to be identical. Therefore, the value of Q for the niobium-containing HSLA grades (2.8 eV) is assumed to be the same as that determined from the literature data [17].

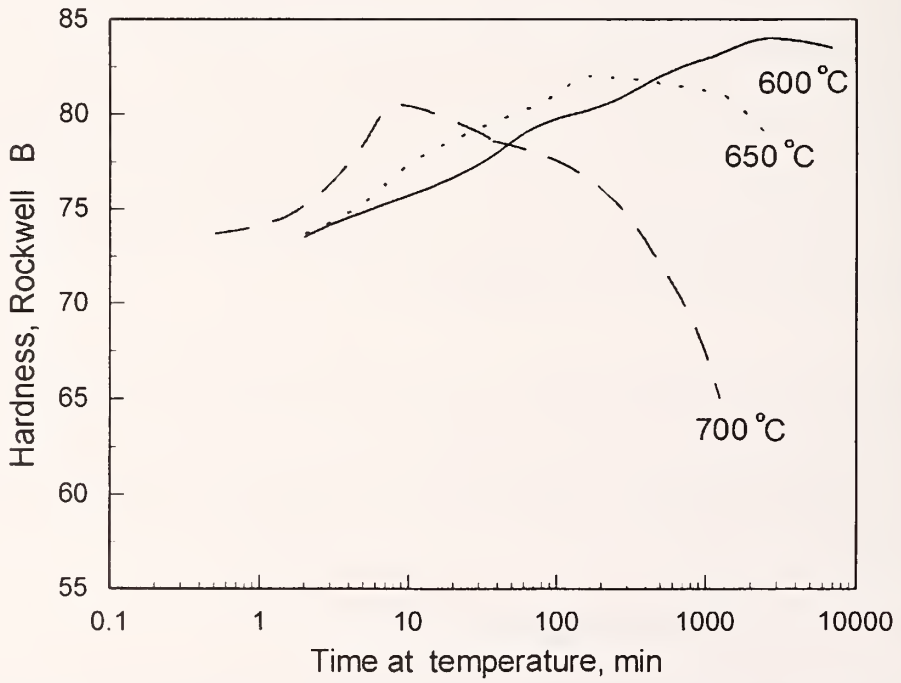

Figure 20. Aging curves for HSLA-V, 350 MPa grade steel as a function of time and temperature.

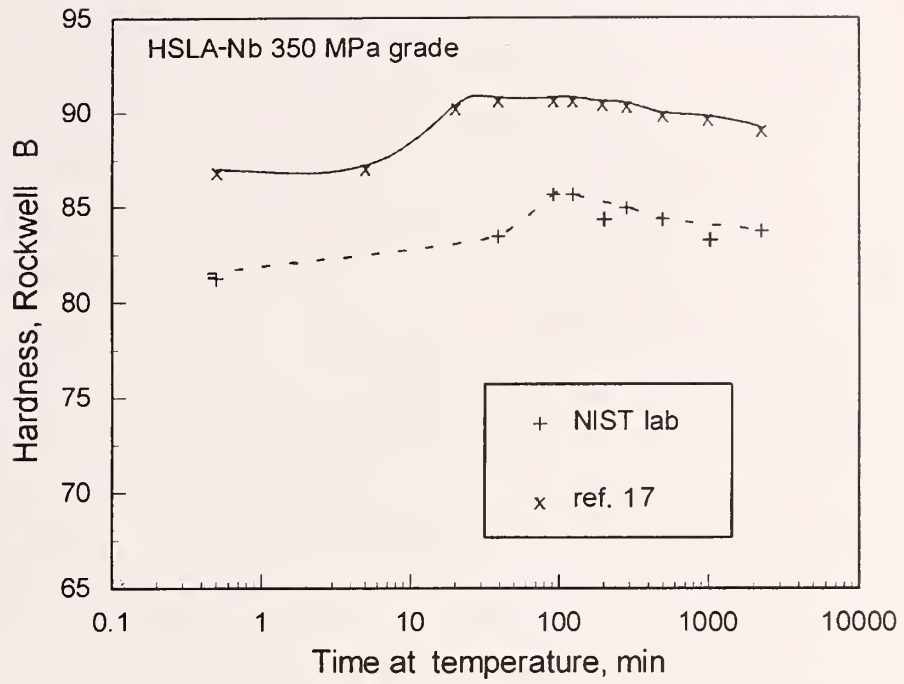

Figure 21. Aging curves for HSLA-Nb steel processing at NIST as a function of time and data from literature [17].

5.2 Fine-Tuning of Equations

Fine-tuning of the structure–property equations goes along with validation of the model and was done in this program so that the accuracy of the model predictions could be maximized. This can be accomplished only when there are sufficient mill data along with metallographic samples to verify the structure.

The best example of fine-tuning is probably the modifications made to the equations for A36. which has a nonpolygonal microstructure. The results from the mill on the thick samples showed us that the predicted UTS was too high compared with the values we measured. The literature data from the ASM handbook of continuous-cooling diagrams [14] contained just enough data to enable a correction for coiling.

A second example of fine-tuning is related to the total elongation in HSLA steel. Given the numerous tests (approximately 70) on the HSLA-Nb steel, we can make a better prediction of the total elongation in the tensile test by simply fitting the data we have rather than basing the prediction on results from a wide variety of low-carbon steel grades. Figure 22 shows the measured total elongation plotted as a function of the measured UTS. The two lines represent the predicted elongation for all steel grades and a revised prediction that better fits the data. The suggested refinement to the prediction reduces the error between prediction and measurement over the range of strengths observed in our tests. In either case, there is a large scatter in the measured elongation for coil samples with UTS between 520 MPa and 560 MPa that no simple refinement in the prediction will resolve. We expect that the morphology of the second phase plays an important role that is not included in the transformation model.

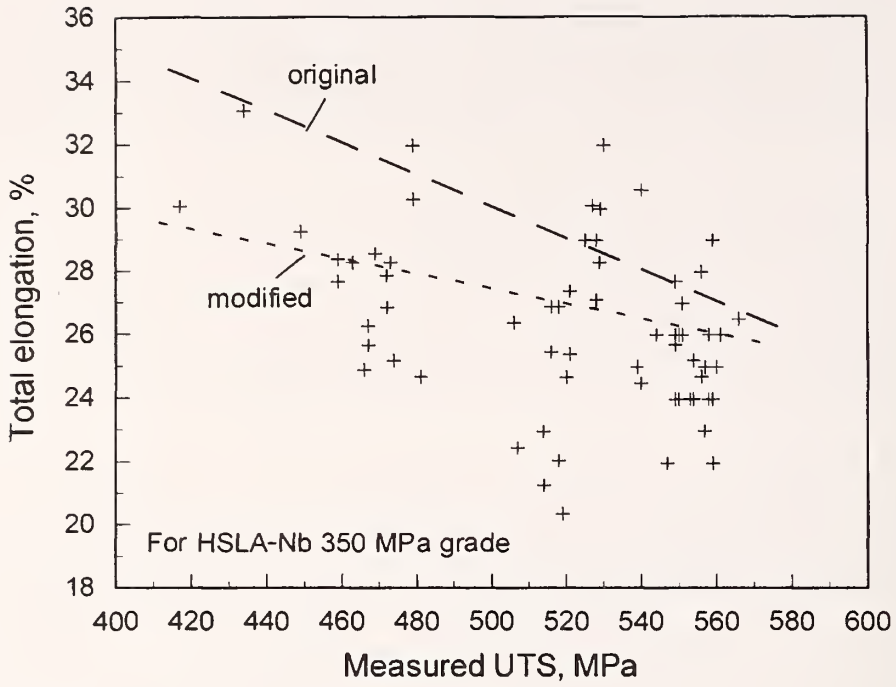

Figure 22. Measured elongation in tensile test as a function of UTS for HSLA-Nb steel.

A third area for fine-tuning is the prediction of UTS for the HSLA-Nb–Ti, 550 MPa grade steel, which has the finest grain size. The data from transformation experiments at UBC indicated that there is a change in the grain-size dependence of hardness (estimated UTS) once the grain size gets below 3.5 $\times 10^{-3}$ mm (see fig. 23). The change in the grain-size dependence for the samples reheated to 1150 °C could be related to the influence of a dislocation substructure, which we have no way to characterize at this point. Therefore, a factor was introduced that adds to the predicted UTS in a linear fashion for grain sizes below 3.5 $\times 10^{-3}$ mm; the difference between the IRSID [3] and modified predictions is zero for a grain size of 3.5 $\times 10^{-3}$ mm and 50 MPa for a grain size of 2 $\times 10^{-3}$ mm.

5.3 Validation of Equations

5.3.1 Plain-Carbon Steel

For A36 and DQSK, we had 14 mill-coil samples or heat-treated samples with measured properties and microstructure (grain size and f_α). A comparison of measured versus predicted properties is shown in figure 24 for the preferred (IRSID) and our alternative choice for equations (Pickering's LYS and Hodgson and Gibbs's UTS). The preferred equations from IRSID showed better agreement with the measured values than the predictions from the alternative equations: the average difference between predicted and measured values was ±20 MPa for the preferred equations; the average difference was ±38 MPa for the alternative equations.

An additional data set supplied by one manufacturer [16] showed quite similar results (fig. 25). The preferred equations from IRSID showed better agreement with the measured values (±15 MPa) than the predictions from the alternative equations (±35 MPa). Therefore, the IRSID equations are preferred to predict the strength properties of plain-carbon steel.

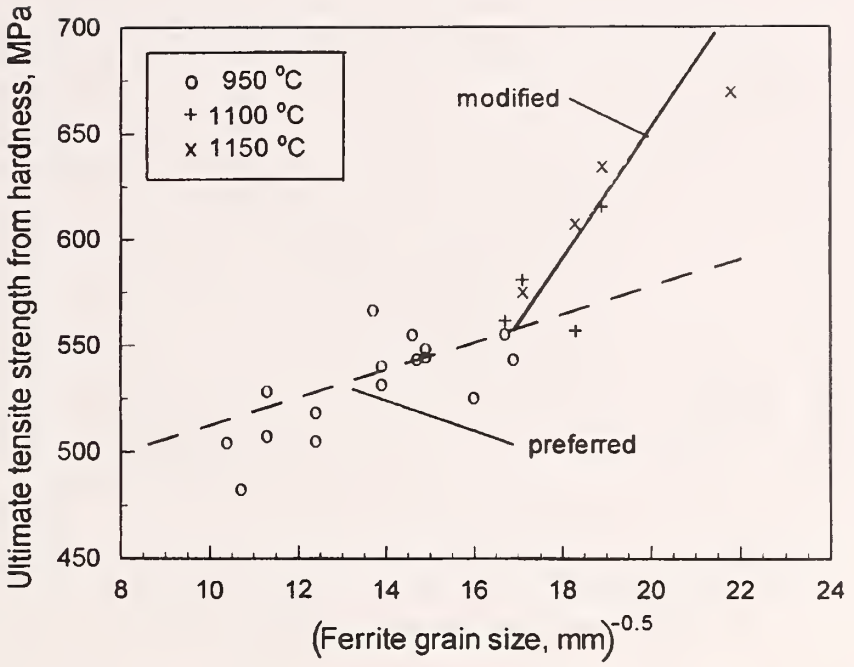

Figure 23. Estimated UTS from transformation experiments conducted at UBC on the HSLA-Nb–Ti, 550 MPa grade steel.

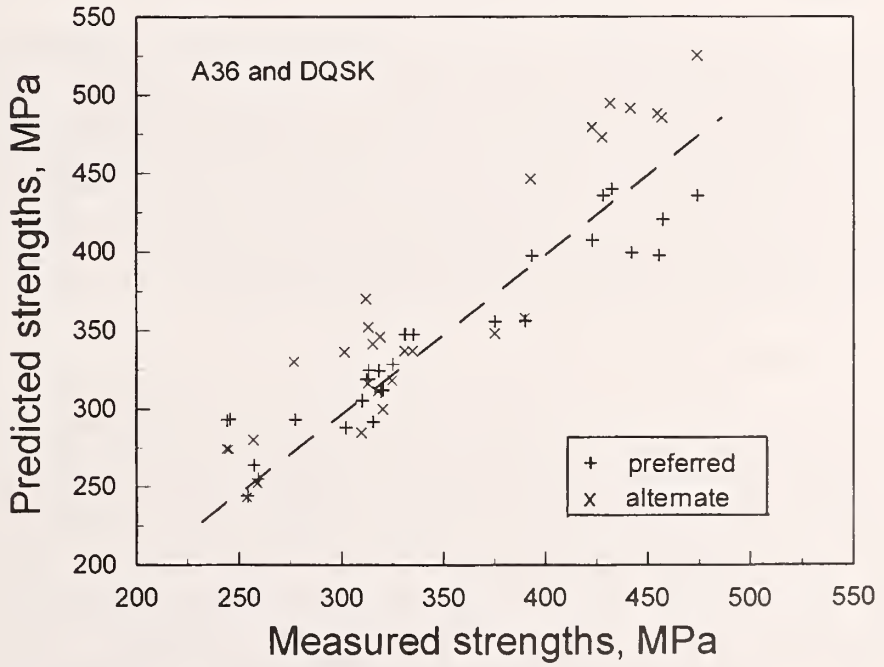

Figure 24. Comparison between measured and predicted properties from both the preferred and alternate equations.

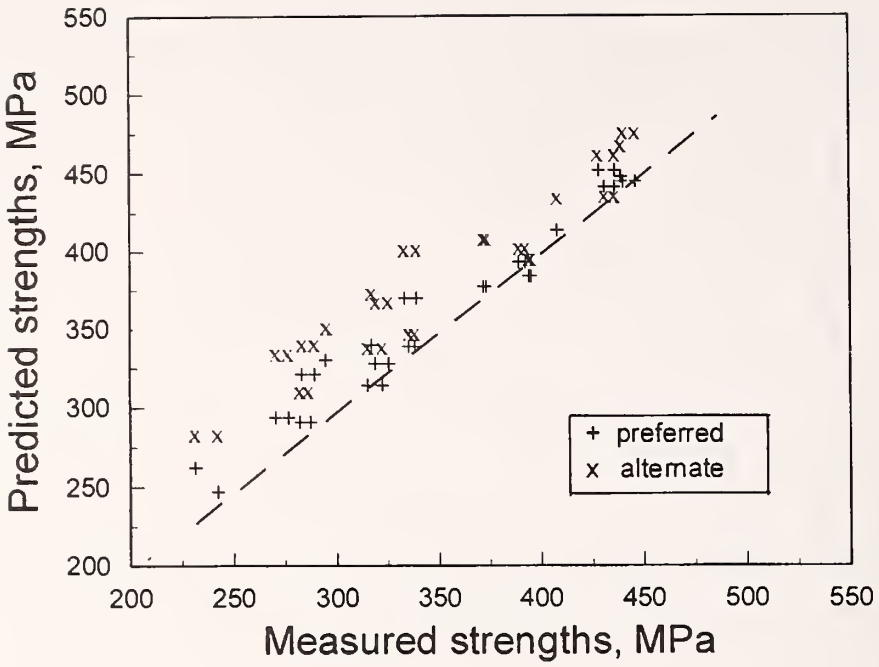

Figure 25. Comparison between measured data from literature [16] and properties predicted by the preferred and alternate equations.

5.3.2 HSLA Steel

The prediction of strength properties in HSLA steel is based on the IRSID equations with the additional factor of precipitation. The precipitation increment is a function of chemical composition and thermomechanical history. Under certain conditions for the niobium-containing HSLA steel grades, strain-induced precipitation can occur in the austenite, which would reduce the niobium content available to precipitate in ferrite where the strengthening occurs. Likewise, the coiling conditions and sample location within the coil can have an influence on precipitation. Both of these factors could lead to a lower precipitation-strengthening contribution. Temper-rolling will reduce the base strength for YS, but not for UTS. All these factors lead to greater uncertainty in the prediction.

5.3.2.1 HSLA-V Grade Steel

For validation purposes, we have determined that the maximum precipitation strengthening for the HSLA-V grade steel (considering the preferred base-strength equations from IRSID) to be 110 MPa for YS and 150 MPa for UTS; for the alternate equations, the maximum strengthening is 100 MPa. The comparison between prediction and measured strength properties for the four coil samples available is shown in figure 26. (The measured LYS of the three temper-rolled coils was increased by 50 MPa to account for temper-rolling.) For the preferred base-strength equation, the prediction was always greater than the measured values. For the alternate equation, there was slightly better agreement between measured and predicted values, particularly for UTS, which is not corrected for temper-rolling.

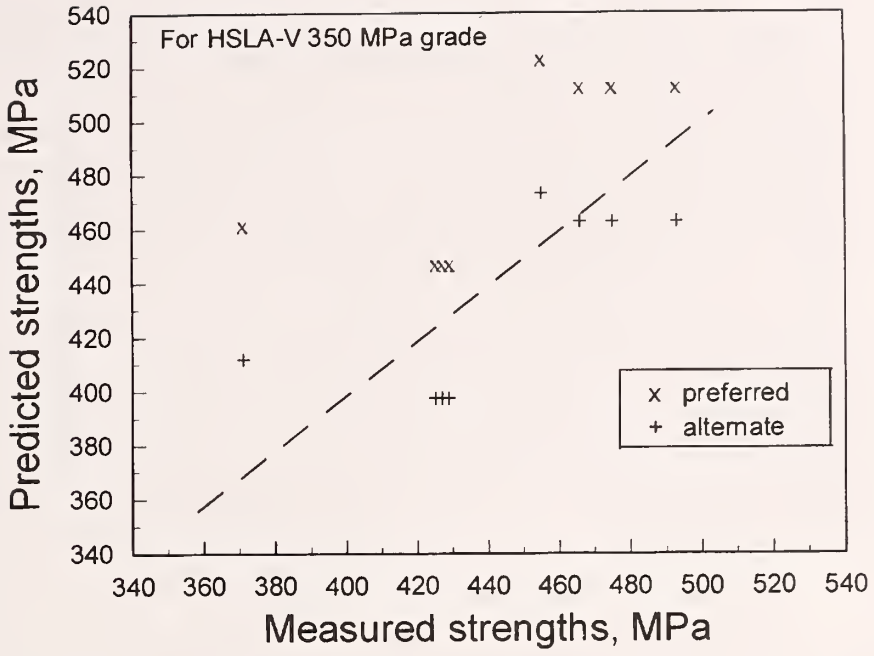

Figure 26. Comparison between HSLA-V, 350 MPa grade steel measured strengths and strengths predicted by both the preferred and alternate equations.

5.3.2.2 HSLA-Nb Grade Steel without Excess Titanium

For validation purposes, we determined the maximum precipitation strengthening for the HSLA-Nb grade steel without excess titanium (considering the preferred base-strength equations from IRSID) to be 150 MPa for coils with 0.04 % niobium and 115 MPa for the coils with 0.023 % niobium. A modification was made to the YS equations so that the YS and UTS increments due to precipitation would be the same. For the alternate equations, the maximum strengthening was assumed to be 100 MPa for the 0.04 % niobium and 70 MPa for the lower niobium grade. The comparison between predicted and measured strength properties for the five coil samples available is shown in figure 27. The agreement between measured and predicted values is excellent for the preferred equations (average difference of 14 MPa) and slightly worse for the alternate equations (average difference of 20 MPa).

5.3.2.3 HSLA-Nb–Ti Grade Steel with Excess Titanium

For validation purposes, we determined that the maximum precipitation strengthening for the HSLA-Nb grade steel (considering the preferred base-strength equations from IRSID) to be 180 MPa; the titanium contribution was 2000 Ti_x where Ti_x is the excess titanium and is equal to the total [Ti] – 3.42[N]. For the alternate equations, the maximum strengthening was assumed to be 150 MPa; the excess titanium contribution was the same. The comparison between predicted and measured strength properties for the three coil samples available is shown in figure 28. The preferred predictions were comparable to the measured properties for all three coils; the alternate equations result in good predictions for two of the three coils.

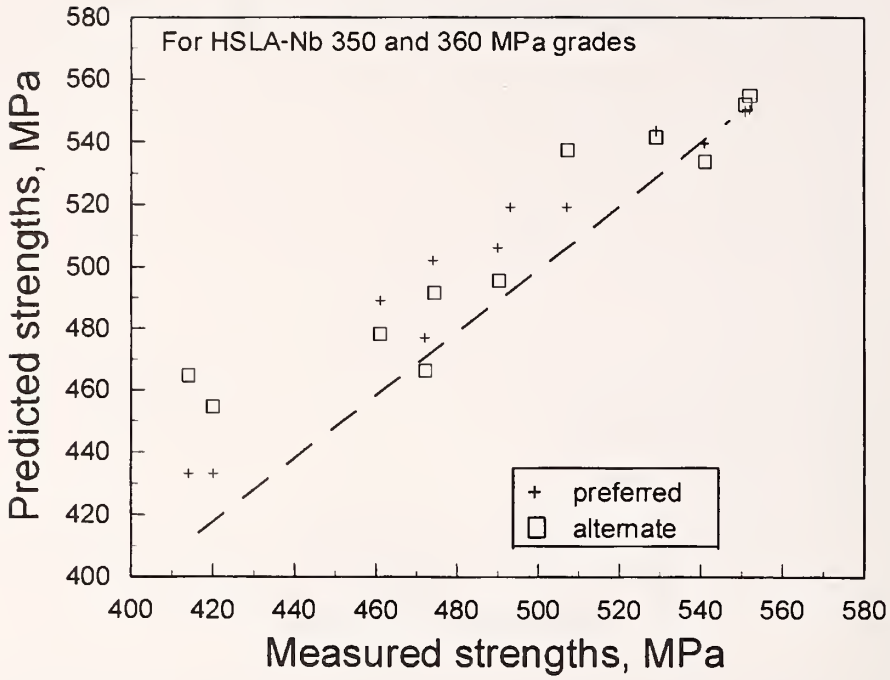

Figure 27. Comparison between measured and predicted properties of HSLA-Nb grade steel without excess titanium.

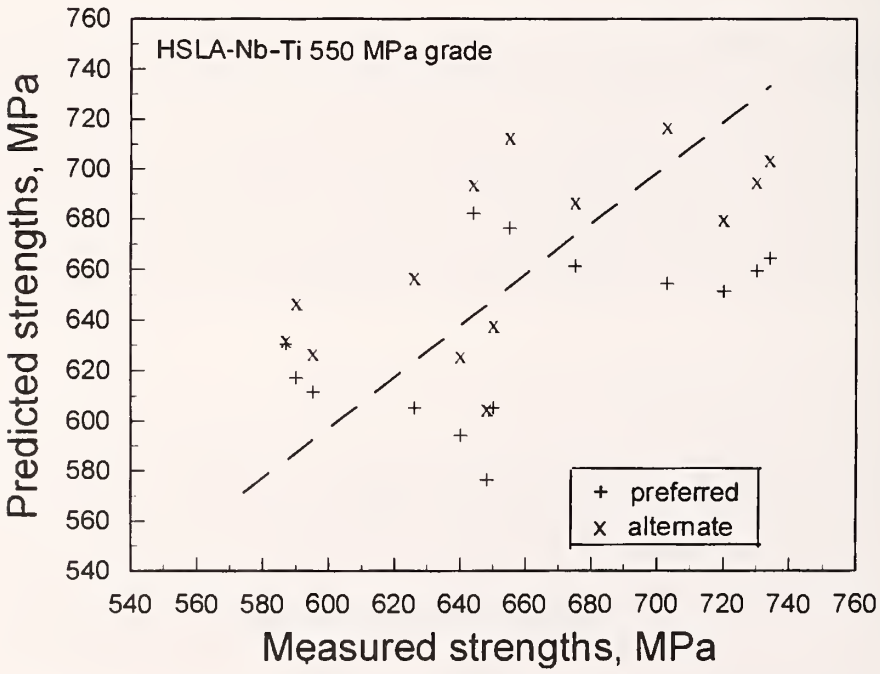

Figure 28. Comparison between HSLA-Nb–Ti measured properties and those predicted by the preferred and alternate equations.

For the HSLA-Nb–Ti, 550 MPa grade steel, we also had an extensive set of mill data (190 coils, 2.5 mm to 5 mm thick) that included processing temperatures, rolling schedule, roll forces, chemical composition, and final properties (LYS, UTS, and total elongation). With no measured ferrite grain size, we had to make some assumptions regarding the microstructure, but some trends were apparent. There was no clear correlation between mechanical properties and coiling temperature (see fig. 29). Possible reasons are (1) the sample for mechanical properties is usually taken at the tail end of the coil where the strength can be reduced by about 30 MPa, depending on the exact position; (2) the variation in the measurement can be ±10 MPa; and (3) chemical composition varies within this grade. The variations in chemical composition were the only ones that we could examine in detail.

Figure 30 shows that the YS increased with higher excess titanium contents (similar to the trend for UTS). The overall trend in the data (2400 MPa per mass percent of excess titanium) had a slightly higher slope than that expected from the literature; that is, excess titanium increased the maximum strength by 2000 MPa per mass percent. The effect of variations in the niobium content within this grade can be considered only when the effect of excess titanium is first subtracted from the measured properties. Figure 31 shows the corrected YS [measured YS – (2000 MPa × the excess titanium] versus niobium content. The variation of niobium from 0.065 % to 0.09 % translates into an apparent increase of about 25 MPa.

After accounting for the composition factors, the scatter in data could still be as large as 100 MPa. The variation due to grain size is the other significant factor that needs to be considered in the prediction. Unfortunately, physical samples do not exist that would enable validation of the grain size in such detail. For the limited coil samples that we received and from the testing of crop samples at UBC, we think that

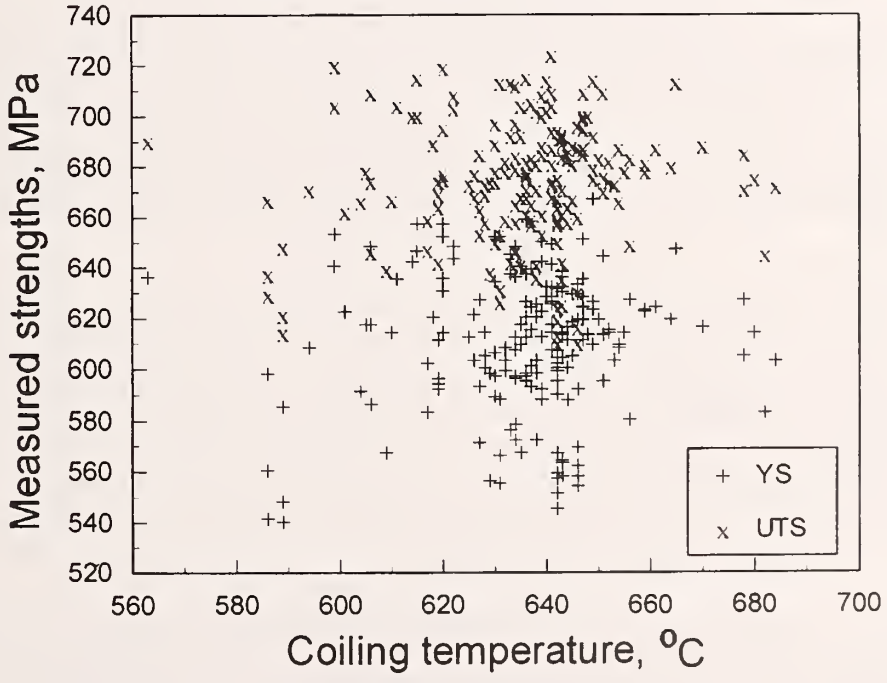

Figure 29. Measured YS and UTS as a function of coiling temperature for the HSLA-Nb–Ti, 550 MPa grade steel.

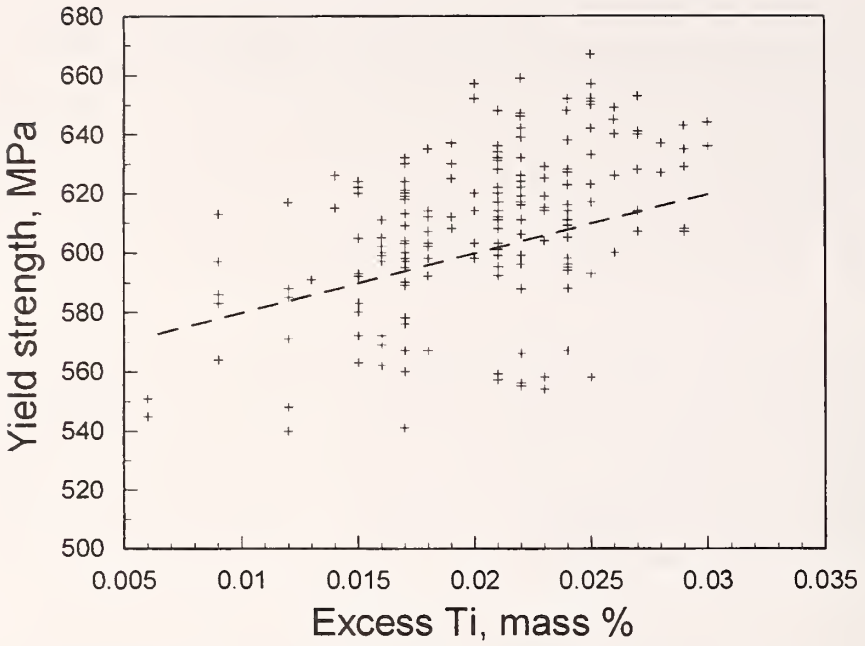

Figure 30. Measured YS as a function of excess titanium in the HSLA-Nb–Ti, 550 MPa grade steel.

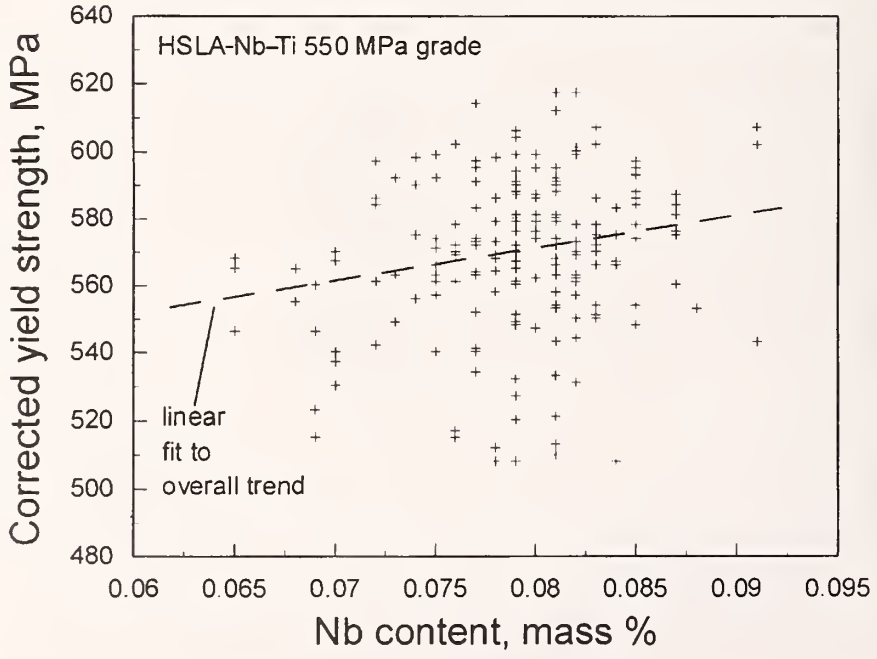

Figure 31. Corrected YS [measured – (2000 MPa × the excess titanium)] as a function of niobium content.

the range of grain sizes that will be produced under typical mill conditions is between 3.5×10^{3} mm and 2×10^{-3} mm. The strengthening contribution predicted from the preferred equations due to grain refinement from 3.5×10^{-3} mm to 2×10^{-3} mm was about 75 MPa; the alternate equations predicted about 80 MPa; both values seem reasonable in light of the measured scatter in data.

In this way, the overall variations in strength can be explained on the basis of variations in chemical composition (titanium, nitrogen, and niobium) and ferrite grain size (transformation characteristics). This prediction scheme appears to be consistent with all the specific data available in the program.

5.3.3 Validation from the Steel Companies

The most thorough validation from a steel company has been the work of Nelson [30]. He studied four grades produced at the mill with chemical compositions most similar to those of materials in our program: A36, DQSK, HSLA-Nb, and HSLA-Nb–Ti, 550 MPa grade steels. In his initial evaluation, the complete program was run on the four grades for various strip thicknesses and finishing and coiling temperatures. A brief summary of the evaluation for the HSLA-Nb, 350 MPa grade steel is shown in table 25. The predicted temperatures at an intermediate location (50 m from the last rolling stand) on the runout table were generally within 50 °C of the measured values. The predicted temperatures at the end of the runout table where the coil enters the downcoiler were often 50 °C to 100 °C lower than the measured values. The YS and UTS predicted by the model were compared with the average values from the grades obtained with similar processing. The agreement between predicted and measured values was typically ±35 MPa, with the predictions scattered equally on either side of the measured values. In general, the model was deemed valuable for testing modifications of the current processing procedures.

From our perspective at NIST, the evaluation of the structure–property equations can be revisited in three areas: (1) The actual chemical compositions for the different grades can be input manually to accurately reflect the solid-solution strengthening in the base strength and the maximum precipitation strengthening. (2) The predicted values of ferrite grain size need to be compared with the measured values when possible. (3) The effect of coiling temperature must be evaluated. In the plain-carbon steels, the coiling temperature affects the contribution from dissolved nitrogen on solid-solution strengthening; for the microalloyed steels, the coiling conditions determine the percentage of precipitation strengthening obtained.

Figure 32 shows the influence of niobium content on the predicted precipitation strengthening. For the HSLA-Nb, 350 MPa grade steel, a range of niobium (about 0.015 % to 0.04 %) can be used to produce the required properties, which translates into a predicted precipitation strengthening of 50 MPa (alternate) or 60 MPa (preferred). The model evaluated by Nelson [30] uses 0.036 % niobium, but the mill-produced samples had only 0.023 % niobium. In other words, if the model used the actual niobium content of the samples instead of the 0.036 % niobium found in the grade used to set up the model, then the predicted strengths would be about 25 MPa lower when the maximum precipitation is predicted from the coiling model.

Figure 33 plots the measured ferrite grain sizes for the as-received samples of this grade as a function of thickness along with the HSMM predictions. The interesting feature here is that the model predicts a minimum ferrite grain size for the sheet at a thickness of about 3 mm. The measured grain sizes seem to indicate that there is a gradual grain refinement with decreasing thickness—to the 1.9 mm thick sample we examined.

Table 25. Summary of HSMM predictions for HSLA-Nb, 350 MPa grade steel.

ID	Thickness, mm	Ferrite grain size, mm	f_α	Δ(coiling temperature)[a] °C	$\Delta\sigma_{pptn}$, MPa	Δ(UTS),[a] MPa
A	2.36	4.2×10^{-3}	—	661/–53	128	—
B	6.49	4.6×10^{-3}	0.93	636/–32	144	+46
C	4.87	4.3×10^{-3}	0.92	657/+8	130	—
D	3.13	3.6×10^{-3}	—	598/+87	153	—
E	12.95	10.1×10^{-3}	0.98	755/–74	56	—
F	1.92	5.1×10^{-3}	0.90	727/–47	74	—
J	4.28	3.9×10^{-3}	—	606/+48	153	+41
K	9.67	6.6×10^{-3}	0.94	641/–2	141	+36
L	3.10	3.4×10^{-3}	0.94	567/+87	143	+30
M	2.13	4.6×10^{-3}	0.93	694/–38	100	–3
N	4.77	4.4×10^{-3}	—	443/+125	50	–58
O	5.31	4.1×10^{-3}	0.94	430/+139	47	–56
P	12.77	7.7×10^{-3}	0.94	567/–11	143	+31

[a] Δ(...) is defined as the difference between the measured value and the HSMM predicted value

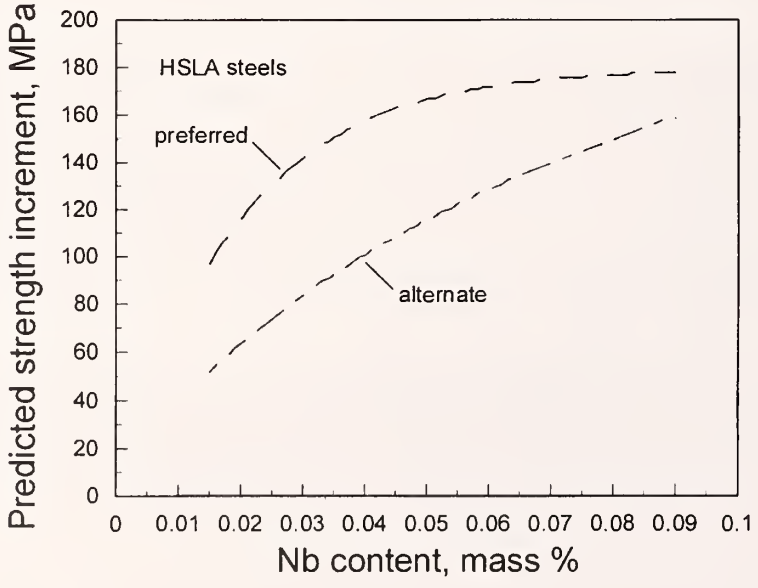

Figure 32. Maximum precipitation strengthening as a function of niobium content.

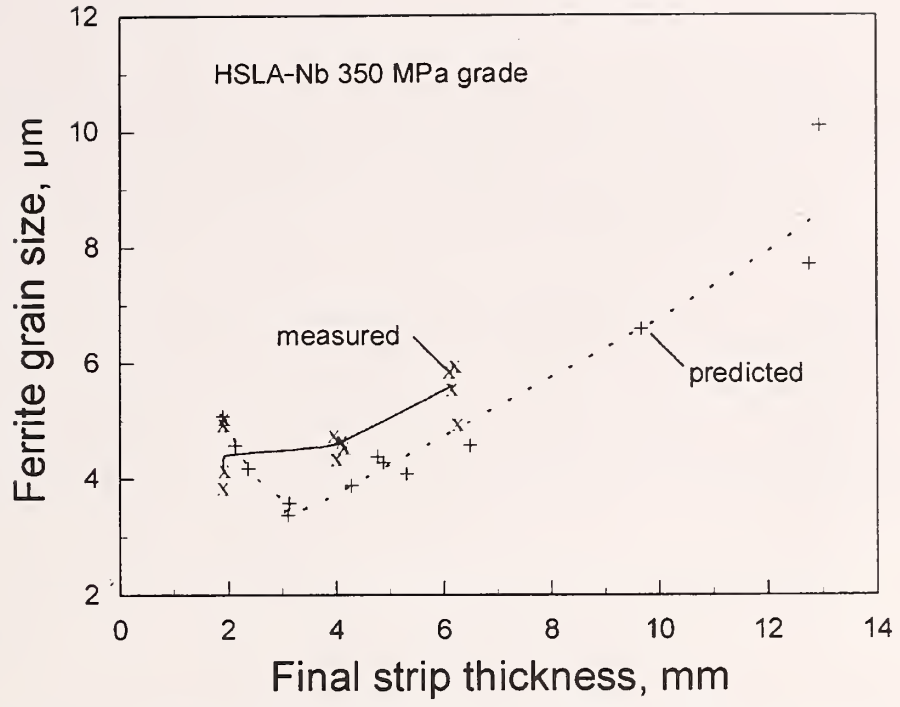

Figure 33. Measured and predicted ferrite grain size [30] versus thickness.

Figure 34 shows the model predictions for free nitrogen in plain-carbon steel and precipitation strengthening in HSLA steel as a function of coiling temperature. The interesting features here are the distinctive shape for each curve; in plain-carbon steel, the free nitrogen predicted from the model (fig. 34a) is a strong function of coiling temperature between about 550 °C and 660 °C. (The model predictions are considered valid for most of the length of the coil, but they may not be valid for the head and tail as well as for the extreme edges.) For temperatures above and below this range, the prediction is not a function of coiling temperature. For example, if the actual coiling temperature were 600 °C and the model predicted a coiling temperature of 650 °C, the model performance would be considered good for the temperature aspect; however, this predicted temperature would lead to a prediction of 10 % free nitrogen, whereas the actual value would be about 65 %. The 55 % difference in free nitrogen means that the predicted strength of a steel containing 0.008 % nitrogen would be inaccurate by about 22 MPa.

A similar exercise can be performed for precipitation strengthening in HSLA steel containing niobium. From figure 34b, the precipitation peaks at 600 °C and drops off to low values on either side of the peak. If the actual coiling temperature were 650 °C, and if the model predicted a coiling temperature of 700 °C, the model performance would be considered good for the temperature aspect. However, a temperature prediction of 700 °C would result in a prediction of 42 % precipitation strengthening, whereas if the temperature prediction for coiling temperature were perfect, the precipitation would be 69 %. The 27 % difference in values would translate into a difference of 11 MPa in the predictions [41 MPa (preferred equation) or 30 MPa (alternate equation)] for a steel with a total of 0.036 % niobium.

(a)

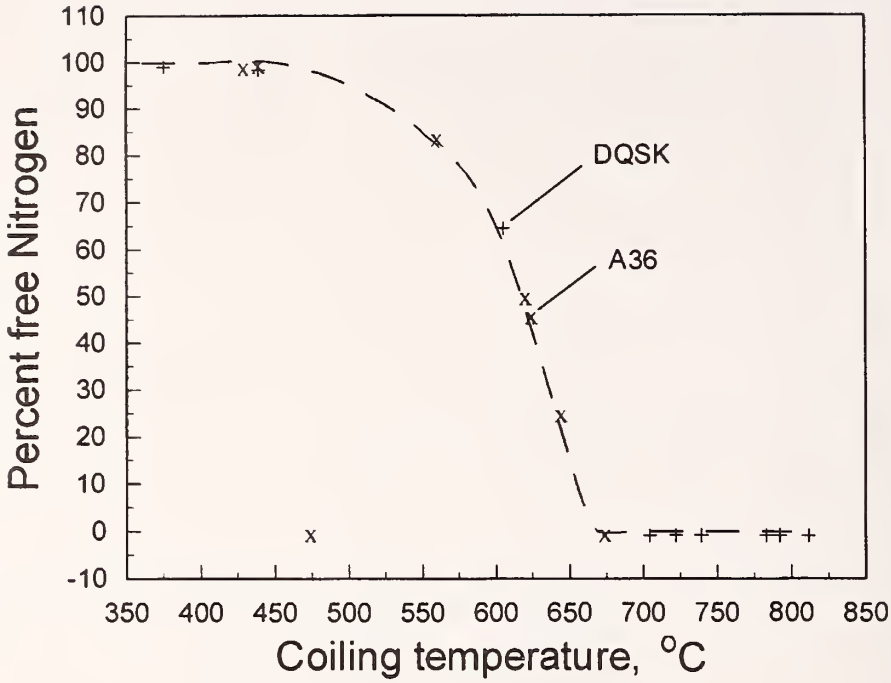

(b)

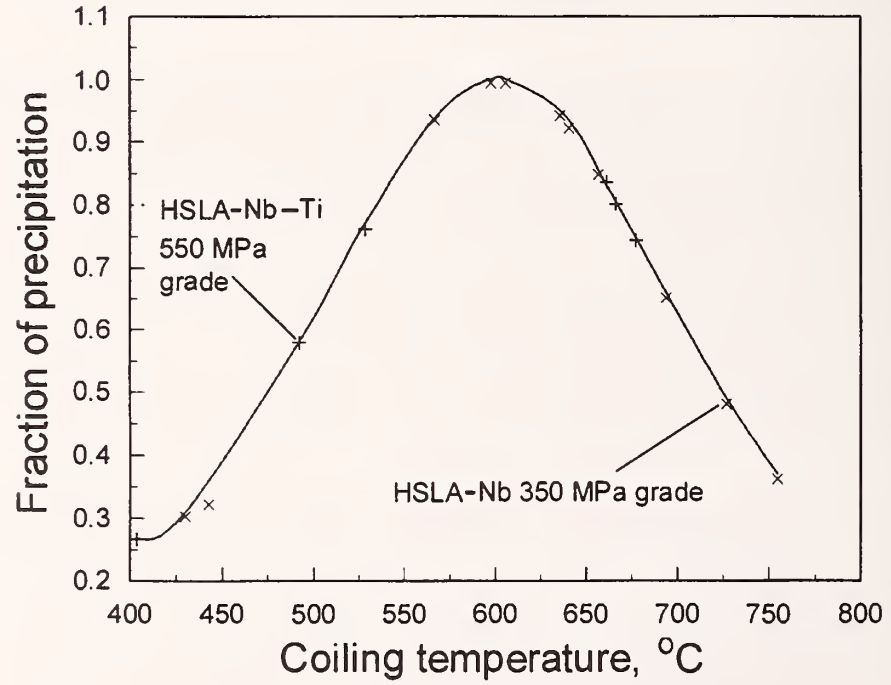

Figure 34. Microstructure predictions from HSMM [30]: (a) fraction of free nitrogen versus coiling temperature; (b) fraction of maximum precipitation strengthening versus coiling temperature.

6. Additional Applications

The proposal anticipated that the model could be applied to a variety of applications other than the hot-strip mill. The best example of this may be the prediction of properties for steel products made on a Steckel mill where the chemical compositions for the steel and processing conditions, the temperature variations, and the interpass times are quite different from those of the hot-strip mill. The preferred equations were used in the program, but they were not validated for Steckel mill products.

For plain-carbon steel in the Steckel mill, little will change in the structure–property equations as long as the steel's matrix structure is predominantly polygonal ferrite. However, in the microalloyed grades, the compositions are often designed to produce additional strength from transformation to acicular microstructures. Also, the maximum precipitation strengthening depends on the soluble microalloy content in the austenite prior to the phase transformation, which varies along the length of the strip from zero to the total microalloy content of the steel. The Shercliff–Ashby process model can be used as in the hot-strip model, except that the maximum strength must be modified to reflect the soluble microalloy content.

7. Limitations

The major limitation in the preferred structure–property equations for general applications appears to be the composition of the steel to be studied. The program has been set up to look at specific steel compositions, and the equations are valid in the range of microstructures typically produced. However, for different combinations of composition and grain size, the equations may give unrealistic predictions. An example can be shown with the HSLA-Nb composition: figure 35 shows the strength predicted by the preferred equations for grain sizes between 2×10^{-3} mm and 14×10^{-3} mm. For grain sizes less than

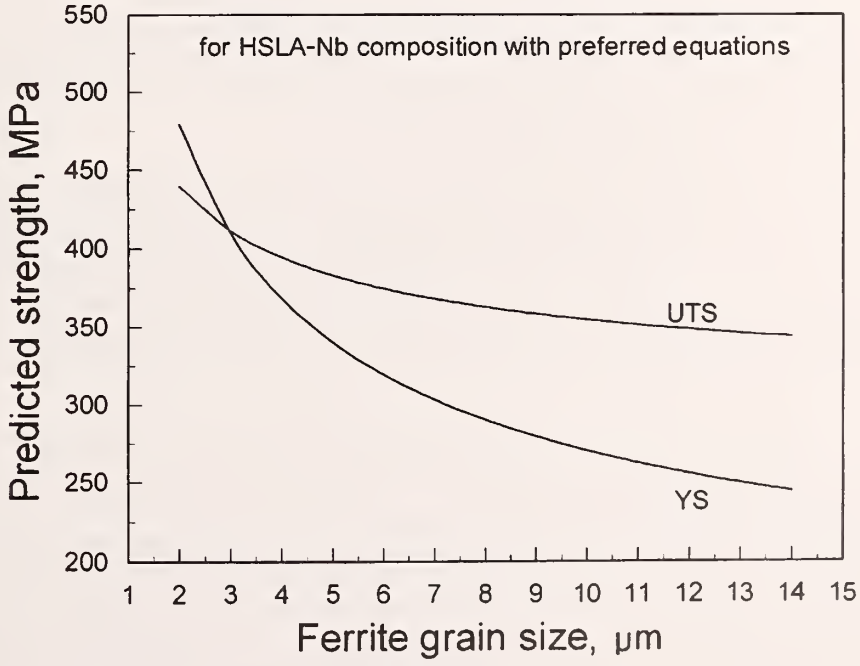

Figure 35. Predicted YS and UTS of HSLA-Nb from the preferred set of equations as a function of grain size.

3×10^{-3} mm, the predicted YS is greater than the predicted UTS, which is unrealistic. With the current processing capability of a hot-strip mill, the grain size will probably be at least 3.5×10^{-3} mm. The predictions for base strength are okay. In the future, with improved equipment and better control of the process, finer grain sizes may be achieved. In general, the preferred equation for YS seems to represent a source of potential problems because grain-size dependence is a function of both carbon and manganese content; this grain-size dependence is absent in the UTS equation.

8. Summary and Recommendations

Equations have been developed and validated for plain-carbon and HSLA steel produced on the hot-strip mill. The lower yield strength, ultimate strength, and percent of total elongation are the main outputs from the equations. For thicker, plate-type products, the DBTT can also be predicted. The accuracy of the HSMM predictions for YS and UTS are critically dependent upon the accuracy of the thermal and transformation models' predictions, which is, at best, ±35 MPa. This is not as good as that reported for a similar model [31], but the HSMM allows for more flexibility and detail in the setup for the hot-strip mill.

Within the context of the goal for our program, the starting assumption was "The differences in properties for a given steel grade can be correlated to microstructure." For the overall trends between grades, there are clearly good correlations between microstructure and properties. On a finer scale, regarding the question of how accurately the properties can be predicted from the microstructure, the answer is less satisfactory. A good example is the HSLA-Nb–Ti, 550 MPa grade steel; figure 12 showed the microstructure from the three different coils. The third coil with the finest measured grain size, which would have the highest predicted strength, had a lower measured strength (about 50 MPa UTS) than the other two. One factor that has not been considered in the prediction of strength is the misorientation across the grain boundaries. All the equations described previously assume that the boundaries are high angle (>20° misorientation).

To obtain a better understanding of misorientation, we did additional studies with a crystallographic orientation mapping system in the SEM. The studies showed that there were several boundaries between grains with nearly the same orientation, even in this equiaxed, polygonal structure. Unfortunately, the technique did not work well with the higher strength HSLA steel.

The equations developed for the structure–property relationships are applicable to a wider range of chemical composition than the eight grades in the program, but, in some cases, the alternate equations (fig. 36) may give better predictions than the preferred equations (fig. 35). Base strength equations are considered applicable to grades in which the microstructure is predominantly polygonal ferrite. Precipitation strengthening can be predicted in steel containing 0.02 % to 0.09 % niobium, 0.08 % vanadium, and excess titanium levels up to 0.025 %.

To improve the applicability of the model in its present form, two areas of additional work related to this subtask appear to be needed. The first is related to the base strength: a systematic approach to correlate base strength to retained austenite and acicular constituents in the microstructure. The second area is related to the Shercliff–Ashby model and its application in the coiling module: more data on precipitate coarsening (activation energy as a function of microalloy content) and measurements of the maximum precipitation strengthening that can be achieved for a given microalloy content. With the additional work, it should be possible to extend the model to predict the properties for all low-carbon steel grades. Future work in this area should consider two additional experimental techniques. First, the use of hardness as a measure of strength could be utilized more extensively than we did in this program. The correlation between hardness and tensile properties is well-known and reasonably accurate, albeit purely empirical. In

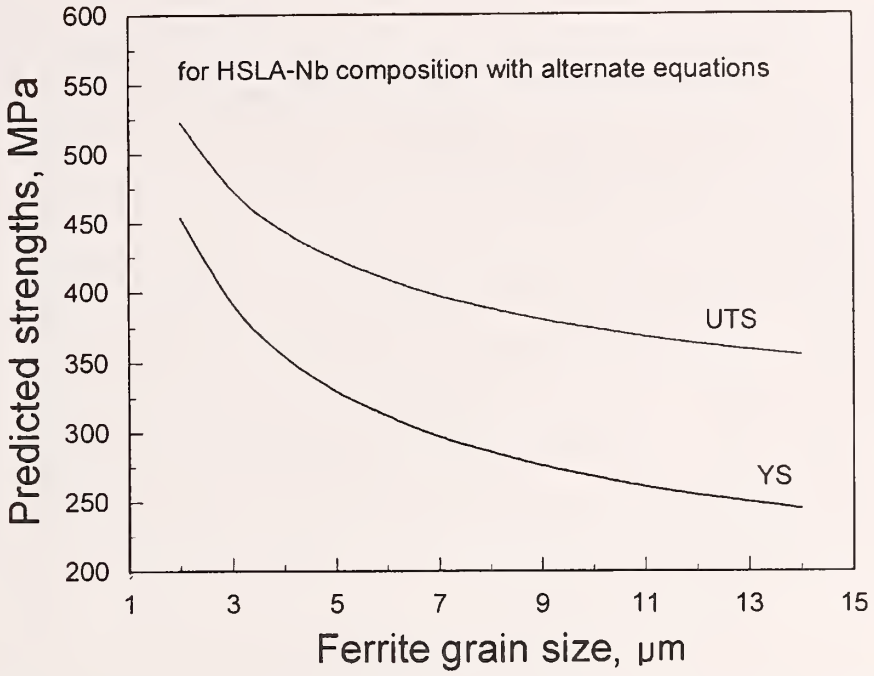

Figure 36. Predicted YS and UTS of HSLA-Nb from the alternate set of equations as a function of grain size.

this program, we developed equations that relate Rockwell B hardness R_B to tensile properties from data supplied by one manufacturer for steel with less than 0.12 % carbon:

$$YS = 386 - 3.23R_B + 0.104R_B^{2.} \quad (14)$$

$$UTS = 586 - 11.3R_B + 0.1255R_B^{2.} \quad (15)$$

The equations were used to predict the strength of hot-rolled coils for automotive applications [32], which was then compared with the measured properties; the results are shown in figure 37. Over the full range of strength properties, the predicted and measured properties agree well.

The other area for refinement in any future test program is related to microstructure characterization. Grain size is a critical factor in the model's predictions of properties. Much of our effort has been in metallographic examination of ferrite grain size, and differences in the measurements made at NIST and at UBC remain, particularly for the HSLA-Nb–Ti, 550 MPa grade steel, which could account for 30 MPa in the prediction. An ultrasonic measurement should provide more consistent values within a given grade. The other project in the Advanced Process Control Project, Online Mechanical Properties Measurement [33], illustrates clearly what an ultrasonic measurement can contribute in the way of characterizing the microstructure. A complimentary magnetic–ultrasonic technique was explored by Igarashi et al. [34] to characterize precipitation in HSLA sheet steel.

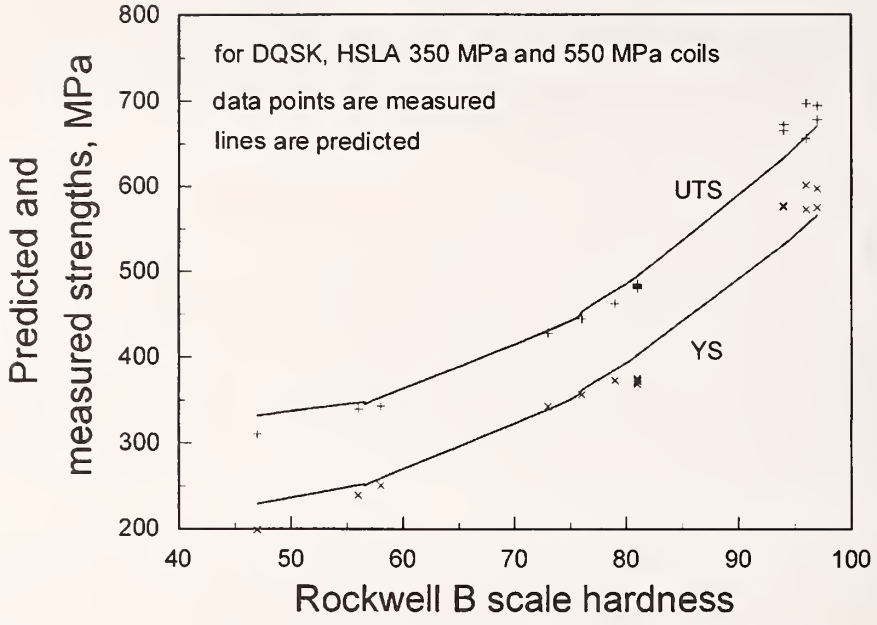

Figure 37. Measured and predicted tensile properties as a function of hardness for DQSK; HSLA, 350 MPa; and HSLA, 550 MPa grade sheet steel for automotive applications.

This work was supported by the American Iron and Steel Institute and performed at NIST under the supervision of G. Alers and H.I. HcHenry. We acknowledge the help with the experimental work we received from R.P. Santoyo and D.P. Vigliotti of NIST. Our partners—P. Repas (U.S. Steel Technical Center), Prof. M. Militzer (University of British Columbia), D. Overby (Stelco), B. Nelson (Dofasco), and W.P. Sun (National Steel)—contributed greatly to our work.

9. References

[1] Hornbogen, E.; Staniek, G. J. Mater. Sci. 9: 879–886; 1974.
[2] Pickering, B.F., in Physical metallurgy and the design of steels. London: Applied Science Publishers; 1978.
[3] Choquet, P.; Fabregue, P.; Giusti, J.; Chamont, B., in Yue, S., ed., Proc. int. symp. on mathematical modeling of hot-rolling of steel. Quebec: ClM; 1990. 34–43.
[4] Suehiro, M.; Sato, K.; Yada, H., Senuma, T.; Shigefuji, H.; Yamshita, Y., in Tamura, I., ed., Int. conf. on physical metallurgy of thermomechanical processing of steels and other metals, THERMEC-88. Tokyo: Iron and Steel Institute of Japan; 1988. 791–798.
[5] Mitchell, P.S.; Morrison, W.B; Crowder, S.N., in Asfahani, R.; Tither, G., eds., Int. Symp. of low-carbon steels for the 90s. Warrendale, PA: The Materials Society; 1993. 337–343.
[6] Kwon, O. Trans. Iron Steel Inst. Jap. 32(12): 350–358; 1992.
[7] Hodgson, P.D.; Gibbs, R.K. Trans. Iron Steel Inst. Jap. 32(12): 1329–1338; 1992.
[8] Tomota, Y.; Umemoto, M.; Komatsubara, N.; Hiramatsu, A.; Nakajima, N.; Moriya, A.; Watanabe, T.; Nanba, S.; Anan, G.; Kunishiga, K.; Higo, Y.; Miyahara, M. Trans. Iron Steel Inst. Jap. 32(12): 343–349; 1992.
[9] Mintz, B. Met. Technol. 11: 265–272; 1984.

[10] Gladman, T.; Pickering, F.B., in Baker, T.N., ed., Yield, flow and fracture of polycrystals. London: Applied Science Publishers; 1983.141–198.
[11] Pickering, F.B., in Cahn, R.W.; Haasen, P.; Kramer, E.J., eds., Materials science and technology—A comprehensive treatment, Vol. 7, Constitution and properties of steels. New York: Wiley–VCH; 1991. 41–94.
[12] Campbell, P.C.; Hawbolt, E.B.; Brimacombe, J.K. Metall. Trans. 22A: 2779–2790; 1991.
[13] DeBray, B.; Teracher, P.; Jonas, J.J. Metall. Trans. 26A: 99–111; 1995.
[14] Atkins, M., ed. Atlas of continuous cooling transformation diagrams for engineering steels. Metals Park, OH: ASM Int.; 1980. 26.
[15] Duit, G.A.; Hurkmans, A.; Scheffer, J.J.F.; Hoogendoorn, T.M., in Tamura, I., ed., Int. conf. on physical metallurgy of thermomechanical processing of steels and other metals, THERMEC-88. Tokyo: Iron and Steel Institute of Japan; 1988. 114–121.
[16] Grozier, J.D., in Microalloying '75. New York: Union Carbide; 1977. 241–250.
[17] Vollrath, L.G.E.; Hackl, R.; Schmitt–Thomas, K.G.; Daub, D., in Microalloying '88. Metals Park, OH: ASM Int.; 1988. 353–358.
[18] Repas, P.E., in Gray, J.M.; Ko, T.; Shoulhua, Z.; Baorong, W.; Xishan, X. eds., HSLA steels, metallurgy and applications. Metals Park, OH: ASM Int.; 1986. 933–940.
[19] Gladman, T.; Dulieu, D.; McIvor, I., in Microalloying '75. New York: Union Carbide; 1977. 32–54.
[20] Melander, A. Scan. J. Met. 7: 109–113; 1978.
[21] Martin, J.W. Micromechanisms in particle-hardened alloys. New York: Cambridge Solid State Science Series; 1980. 61.
[22] Gawne, D.T.; Lewis, G.M.H. Mater. Sci. Techol. 1: 183–191; 1985.
[23] Parilák, L.; Šlesár, M.; Štefan, B., in Microalloying '88, Metals Park, OH: ASM Int.; 1988.559–569.
[24] Österle, W., in Proc. HSLA steels conference. Beijing; 1995. 243–246.
[25] Kwon, O., in Microalloying '95. Warrendale, PA: Iron and Steel Society; 1995. 251–262.
[26] Purtscher, P.T.; Cheng, Y.; Kuziak, R.; Foley, R.P., in Proc., 37th MWSP conf., vol. XXXIII. Warrendale, PA: Iron and Steel Society; 1996. 405–416.
[27] AISI–UBC–NIST project "Microstructural engineering in hot-strip mills," Subtasks C2.5 and C2.6. Annual progress report; May 1995 and 1996.
[28] Zajac, S.; Siwecki, T.; Korchynsky, M., in Asfahani, R.; Tithere, G., eds., Proc., Int. symp. of low-carbon steels for the 90s. Warrendale, PA: The Materials Society; 1993.139–149.
[29] Shercliff, H.R.; Ashby, M.F. Acta Metall. Mater. 38(10): 1789–1812; 1990.
[30] Nelson, B. Presentation at IISI TECHO-30, Washington, April 28, 1998.
[31] Nanba, S. et al. Kobelco Technol. Rev., No. 21, April 1998. 3–6.
[32] Mackie, T. Private communication: AISI Auto-Steel Partnership data.
[33] Chase, V. R&D Magazine, pp. 39–43; May 1996.
[34] Igarashi, B.; Alers, G.; Purtscher, P.T. 1997 ASNT spring conf./Sixth annual research symp., Houston, TX. Columbus, OH: American Society for Nondestructive Testing; 1997

*U.S. GPO 1999-0-773-022/40147

NIST Technical Publications

Periodical

Journal of Research of the National Institute of Standards and Technology—Reports NIST research and development in those disciplines of the physical and engineering sciences in which the Institute is active. These include physics, chemistry, engineering, mathematics, and computer sciences. Papers cover a broad range of subjects, with major emphasis on measurement methodology and the basic technology underlying standardization. Also included from time to time are survey articles on topics closely related to the Institute's technical and scientific programs. Issued six times a year.

Nonperiodicals

Monographs—Major contributions to the technical literature on various subjects related to the Institute's scientific and technical activities.

Handbooks—Recommended codes of engineering and industrial practice (including safety codes) developed in cooperation with interested industries, professional organizations, and regulatory bodies.

Special Publications—Include proceedings of conferences sponsored by NIST, NIST annual reports, and other special publications appropriate to this grouping such as wall charts, pocket cards, and bibliographies.

Applied Mathematics Series—Mathematical tables, manuals, and studies of special interest to physicists, engineers, chemists, biologists, mathematicians, computer programmers, and others engaged in scientific and technical work.

National Standard Reference Data Series—Provides quantitative data on the physical and chemical properties of materials, compiled from the world's literature and critically evaluated. Developed under a worldwide program coordinated by NIST under the authority of the National Standard Data Act (Public Law 90-396). NOTE: The Journal of Physical and Chemical Reference Data (JPCRD) is published bimonthly for NIST by the American Chemical Society (ACS) and the American Institute of Physics (AIP). Subscriptions, reprints, and supplements are available from ACS, 1155 Sixteenth St., NW, Washington, DC 20056.

Building Science Series—Disseminates technical information developed at the Institute on building materials, components, systems, and whole structures. The series presents research results, test methods, and performance criteria related to the structural and environmental functions and the durability and safety characteristics of building elements and systems.

Technical Notes—Studies or reports which are complete in themselves but restrictive in their treatment of a subject. Analogous to monographs but not so comprehensive in scope or definitive in treatment of the subject area. Often serve as a vehicle for final reports of work performed at NIST under the sponsorship of other government agencies.

Voluntary Product Standards—Developed under procedures published by the Department of Commerce in Part 10, Title 15, of the Code of Federal Regulations. The standards establish nationally recognized requirements for products, and provide all concerned interests with a basis for common understanding of the characteristics of the products. NIST administers this program in support of the efforts of private-sector standardizing organizations.

Consumer Information Series—Practical information, based on NIST research and experience, covering areas of interest to the consumer. Easily understandable language and illustrations provide useful background knowledge for shopping in today's technological marketplace.
Order the **above** *NIST publications from: Superintendent of Documents, Government Printing Office, Washington, DC 20402.*
Order the **following** *NIST publications—FIPS and NISTIRs—from the National Technical Information Service, Springfield, VA 22161.*

Federal Information Processing Standards Publications (FIPS PUB)—Publications in this series collectively constitute the Federal Information Processing Standards Register. The Register serves as the official source of information in the Federal Government regarding standards issued by NIST pursuant to the Federal Property and Administrative Services Act of 1949 as amended, Public Law 89-306 (79 Stat. 1127), and as implemented by Executive Order 11717 (38 FR 12315, dated May 11, 1973) and Part 6 of Title 15 CFR (Code of Federal Regulations).

NIST Interagency Reports (NISTIR)—A special series of interim or final reports on work performed by NIST for outside sponsors (both government and non-government). In general, initial distribution is handled by the sponsor; public distribution is by the National Technical Information Service, Springfield, VA 22161, in paper copy or microfiche form.

U.S. Department of Commerce
National Institute of Standards and Technology
325 Broadway
Boulder, Colorado 80303-3337

Official Business
Penalty for Private Use, $300